Journal of African Earth Sciences 60 (2011) 133–152

Contents lists available at ScienceDirect

Journal of African Earth Sciences

journal homepage: www.elsevier.com/locate/jafrearsci

Eburnean and Pan-African granitoids and the Raghane mega-shear zone evolution: Image analysis, U–Pb zircon age and AMS study in the Arokam Ténéré (Tuareg shield, Algeria)

O. Nouar [a], B. Henry [b,*], J.P. Liégeois [c], M.E.M. Derder [a], B. Bayou [a], O. Bruguier [d], A. Ouabadi [e], M. Amenna [a], A. Hemmi [a], M. Ayache [a]

[a] CRAAG, BP 63, 16340 Bouzaréah, Alger, Algeria
[b] Paléomagnétisme, IPGP, PRES Sorbonne Paris Cité and CNRS, 4 avenue de Neptune, 94107 Saint-Maur cedex, France
[c] Isotope Geology, Royal Museum for Central Africa, B-3080 Tervuren, Belgium
[d] Géosciences Montpellier, Université de Montpellier II, 34095 Montpellier, France
[e] Laboratoire "Géodynamique, Géologie de l'Ingénieur et Planétologie", FSTGAT/USTHB, BP 32, El-Alia Bab Ezzouar, 16111 Alger, Algeria

ARTICLE INFO

Article history:
Received 12 October 2010
Received in revised form 7 February 2011
Accepted 11 February 2011
Available online 17 February 2011

Keywords:
Eburnean
Pan-African
Saharan metacraton
Shear zone
Anisotropy
Magnetic susceptibility
Remote sensing
U–Pb zircon age

ABSTRACT

In the Arokam Ténéré, the three studied massifs of granitoids are located around the N–S oriented Raghane mega-shear zone, which separates two of the main domains of the Tuareg shield, the Saharan metacraton and the Central Hoggar. The field observations, AMS analyses and U–Pb zircon dating were completed by a study of Landsat images because of the scarcity of outcrops in several parts of the studied area.

The image analysis allows to distinguish Arokam-East and Abdou granitoids in the eastern plutonic complex. It has also shown that the western plutonic complex corresponds to two different intrusions: the Yvonne granite and granodiorite. This is confirmed by the magnetic fabric that presents different characteristics in the different granitoids. U–Pb zircon dating and field observations show that the Arokam-West basement granite is much older (1915 Ma) than the Hanane granodiorite (582 Ma) in the central plutonic complex. Arokam-East and -West granites then belong to the Eburnean basement. The magnetic fabric of these granites is mainly associated with a post-magmatic deformation, probably of Pan-African age. Yvonne granodiorite is likely contemporaneous of the main displacement along the Raghane shear zone. The Yvonne granite (594 Ma) and Hanane granodiorite have a fabric similar to that previously obtained in most plutons of the Tririne area. This fabric is related to the regional stress field, associated with the activity of the Raghane shear zone, during the late-magmatic phase in the plutons. On the contrary, the magnetic fabric of the Abdou pluton is still reflecting only the magma flow.

1. Introduction

The Raghane – also called 8°30′ – shear zone (Liégeois et al., 1994), one of the most important structures in Africa, crosses the entire Hoggar in Algeria and the Aïr in Niger. These two regions belong to the Tuareg shield, a more than half million square km of Precambrian basement surrounded by Phanerozoic sediments (Fig. 1). The Raghane shear zone (RSZ) separates two different domains, each being composed of several terranes (Black et al., 1994). To the west of RSZ, the Hoggar terranes are mainly composed of Archean and Paleoproterozoic rocks variably affected by the Pan-African orogeny (630–580 Ma; Bertrand et al., 1986; Liégeois et al., 1994, 1998, 2003). Formerly known as Central Hoggar (Lelubre, 1952), it is now known as the LATEA microcontinent, the acronym of its constituent terranes, Laouni, Azrou n'Fad, Tefedest, Egéré-Aleksod and Assodé-Issalane (Liégeois et al., 2003; Liégeois, 2005). LATEA is considered as a metacraton (Abdelsalam et al., 2002; Liégeois et al., 2003), i.e. an Archean-Paleoproterozoic basement variably affected by the Pan-African orogeny (mainly marked by large batholith – Bertrand et al., 1986; Acef et al., 2003 – and high-temperature metamorphism) but leaving nearly intact large tract of the basement (Bendaoud et al., 2008). To the east of RSZ, four terranes have been described. In Aïr, the Barghot terrane comprises Archean and Paleoproterozoic rocks affected by the main Pan-African phase and is covered by 730–660 Ma oceanic rocks of the Aouzegueur terrane (Liégeois et al., 1994) also present in Algerian Hoggar (Caby and Andreopoulos-Renaud, 1987). Recently, Fezaa et al. (2010) have shown that the two easternmost Hoggar

* Corresponding author. Tel.: +33 1 45 11 41 83; fax: +33 1 45 11 41 90.
E-mail addresses: obnouar@hotmail.com (O. Nouar), henry@ipgp.fr (B. Henry), jean-paul.liegeois@africamuseum.be (J.P. Liégeois), mderder58@yahoo.fr (M.E.M. Derder), bbayou57@yahoo.fr (B. Bayou), olivier.bruguier@gm.univ-montp2.fr (O. Bruguier), ouabadi@yahoo.fr (A. Ouabadi).

1464-343X/$ - see front matter © 2011 Elsevier Ltd. All rights reserved.
doi:10.1016/j.jafrearsci.2011.02.007

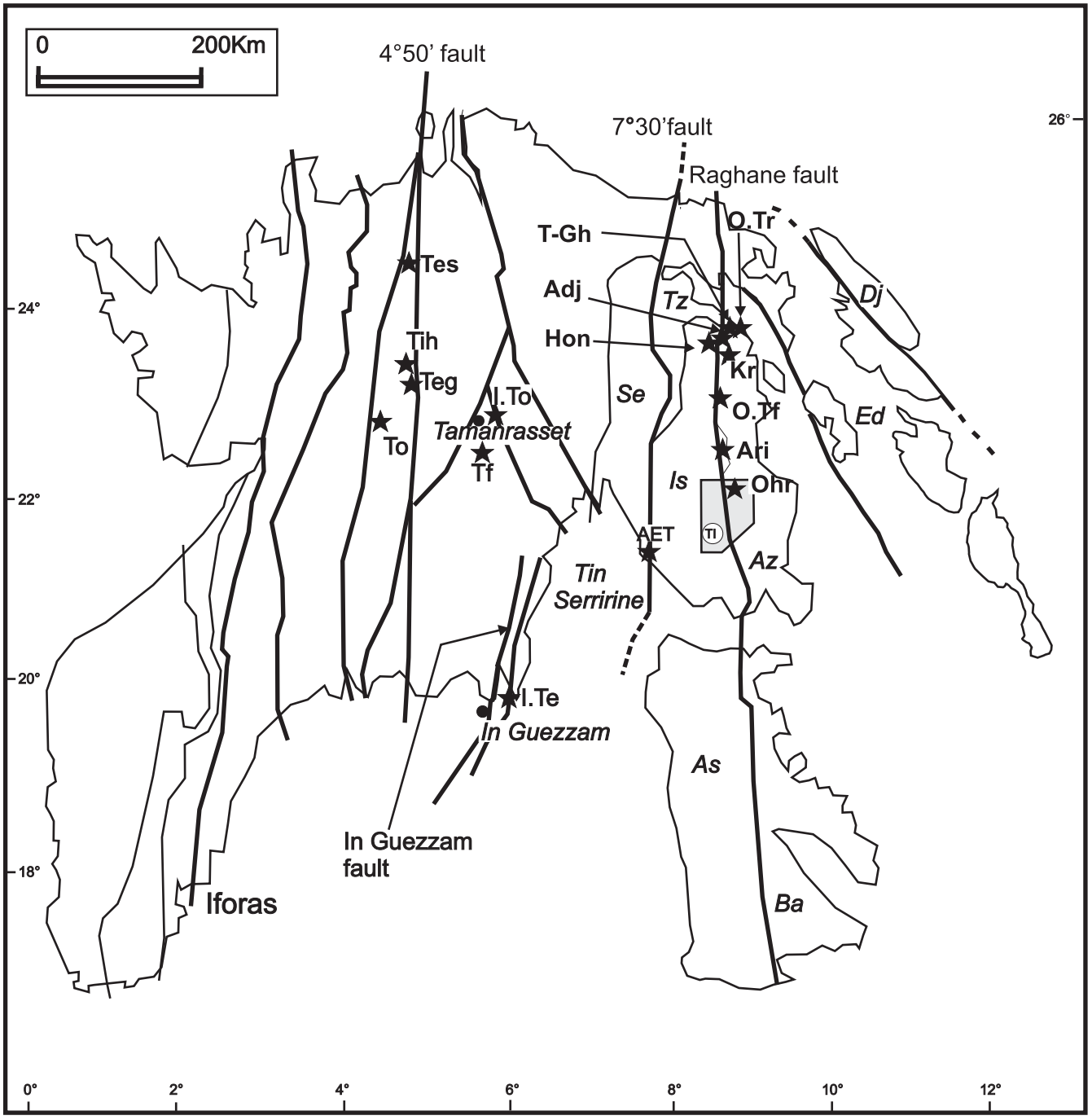

Fig. 1. Geological sketch map of the Hoggar shield showing the previously studied Late Pan-African plutons. Terranes of Assodé – As, Issalane – Is, Tazat – Tz, Aouzegueur – Az, Barghot – Ba, Djanet – Dj and Edembo – Ed. Tihaliouine – Tih, Teg Orak – Teg (Henry et al., 2008), Tesnou – Tes (Djouadi and Bouchez, 1992), Alous En Tides – AET (Henry et al., 2004), In Telloukh – Ite (Henry et al., 2007), Tioueine – To (Djouadi et al., 1997), Tifferkit – Tf, In Tounine – Ito (Henry et al., 2006), Tin Ghoras – TGh, Oued Tiririne, – OTr, Honag – Hon, Adjou – Adj, Kerkour – K r, Oued Touffok – Otf, Arigher – Ari and Ohergehem – Ohr (Henry et al., 2009). Arokam Ténéré study– TI.

terranes, Djanet and Edembo, have been affected by the intracontinental Murzukian episode, between 575 and 555 Ma, an event unknown to the west of the RSZ, except as brittle tectonics, quartz dykes and very late and localized upper level circular plutons (Fezaa et al., 2010). The Arigher batholith within the Aouzegueur terrane also belongs to this orogenic phase (Henry et al., 2009). By contrast, the main Pan-African phase (630–580 Ma) is absent to the east of the RSZ (Fezaa et al., 2010), except in its immediate vicinity (Henry et al., 2009), preserving the Tiririne sedimentary Group from any important deformation, except to the NW, along the Raghane shear zone (Bertrand et al., 1978). The main orientation of the Murzukian structures are oriented NW–SE (Fig. 1), probably along pre-existing Eburnean structures (Fezaa et al., 2010) while the shear zones to the west of the RSZ are mostly oriented N–S (Black et al., 1994). The terranes to the east of the RSZ, eastern Hoggar and eastern Aïr, belong to the Saharan metacraton (Liégeois et al., 1994; Fezaa et al., 2010). The RSZ actually constitutes the western boundary of the Saharan metacraton (Abdelsalam et al., 2002). A geological map showing the different generations of granitoids does not still exist. Available geological maps (Vialon and Guérangé, 1959; Arène et al.,

1961; Bertrand et al., 1978; Fomine, 1990) only distinguish plutons as a whole from their host-rocks that were the subject of a more detailed cartography. To the west of RSZ, the Assodé-Issalane terrane displays an Eburnean basement affected by a high-temperature amphibolite-facies Pan-African metamorphism accompanied by large batholiths and later circular plutons, all within the 630–580 Ma age range (Liégeois et al., 1994).

Close to the Raghane shear zone, the different episodes can be present: the still poorly known probably ocean-related old events at *c.* 790, 730 and 660 Ma, the 630–580 Ma phase related to the collision with the West African craton and the 575–555 Ma phase related to the collision with the Murzuq craton, in the addition to the Eburnean basement known to the south in Niger (Liégeois et al., 1994). This paper aims to better understand this complex Pan-African evolution of the Raghane mega-shear zone by analyzing the structure of different plutons using the anisotropy of magnetic susceptibility (AMS) method (e.g. King, 1966; Hrouda et al., 1971; Henry, 1974; Djouadi and Bouchez, 1992; Archanjo et al., 1994; Borradaile and Kehlenbeck, 1996; Pignotta and Benn, 1999; Bouchez, 2000; Tomezzoli et al., 2003; Henry et al., 2004; Auréjac et al., 2004; Kratinová et al., 2007; Georgiev et al., 2009; Njanko et al., 2009) on plutons adequately dated by the U–Pb method on zircon. This represents the complement of a previous study performed in the northern areas of the Raghane shear zone, notably in the Hassi Tiririne and Tadoumet areas (Henry et al., 2009). For these previously studied plutons, the AMS records the regional stress field during their late magmatic stage or a post-magmatic deformation according to the cases. Detailed image analysis completes the present study, by specifying the geological edges of the plutons because of the scarcity of outcrops in parts of the studied area.

2. Geological setting of the studied area

To the north of the studied area, in the Hassi Tiririne and Tadoumet areas, three magmatic suites at 793 Ma (Oued Touffok pluton in an old tectonic sliver; Fig. 1), 594 Ma (Ohergehem pluton; Fig. 2) and 554 Ma (Arigher batholith; Fig. 1) are located along the Raghane shear zone (Zeghouane, 2006; Zeghouane et al., 2008; Henry et al., 2009). No pre-Neoproterozoic basement was known in the area before this study but abundant Eburnean ages have been obtained on detrital zircons to the east in the Djanet Group, considered as the equivalent of the Tiririne Group (Fezaa et al., 2010).

The studied area (Fig. 2) is located within the "Mont du Métal" 1/200,000 geological map (Vialon and Guérangé, 1959), corresponding to the present topographical map "Timoleitine".

To the east of the RSZ, within the Saharan metacraton, the Arokam Ténéré corresponds mainly to the detritic Tiririne Group, probably deposited between 590 and 570 Ma by comparison with the Djanet Group (Fezaa et al., 2010). The detritic Tiririne Group is a molassic material beginning by a basal polygenic conglomerate overlain by silts and sandstones alternations (Blaise, 1961; Bertrand et al., 1978). In this area, the Tiririne Group is nearly devoid of metamorphism.

Below the Tiririne Group, granites and orthogneisses are present. The Ohergehem pluton, 594 ± 4 Ma old, displays a strong visible fabric, which developed during the crystallization of the magma and which coincides with the magnetic fabric (Henry et al., 2009). Its foliation is globally N–S while its stretching lineation is NE–SW with a plunge of 60° to the SW, interpreted as corresponding to an east-verging thrust tectonics associated with the large transpressive movements that occurred along the Raghane shear zone. This interpretation is in agreement with that given to the south in Aïr for the Dabaga-East plutons (Liégeois et al., 1994, 1998). Here we focus on two areas characterized by an orthogneiss (Arokam-East and -West; Fig. 2) and two plutons (Hanane and Abdou; Fig. 2), Hanane being intrusive in the Arokam orthogneiss.

In addition, we study also the Yvonne pluton (Fig. 2), intrusive in the Assodé-Issalane terrane, to the west of RSZ for comparison purpose as its structure is similar to that of Hanane and Abdou plutons. It is a high-level pluton, macroscopically undeformed and sharply cutting its country-rocks. Its basement is a metamorphic complex made of amphibolites and gneisses, characterized by a high-temperature metamorphism (6 ± 1 kbar and 700 °C for the primary paragenesis to 4 ± 1 kbar and 600 °C for the secondary paragenesis) and the abundance of migmatites (Liégeois et al., 1994).

3. Field and laboratory observations and image analysis

A remote sensing study completed the classical structural and petrographical observations made on the field in the studied sites (Fig. 3) and in the laboratory. The used satellite images are taken from a Landsat scene: path and row 190–45 of 2000/11/19. Specific enhancement processing has been done to precise edge and shape of the studied complexes.

3.1. The Arokam-West orthogneiss

This massif is a drop-shaped N–S oriented massif, located about 6 km east of the Raghane mega shear-zone (Fig. 2). This shape results from erosion, which affected the overlying Tiririne Group. This massif is indicated as a syntectonic granite in the BRMA geological map of "Mont du Métal" (Vialon and Guérangé, 1959), in agreement with its orthogneiss nature. The Arokam-West protolith is mainly constituted by pink middle-grained, calc-alkaline biotite granite with dark elongated enclaves. On the southwestern part of the Arokam-West massif, mixing-mingling patterns between granite and gabbro-diorite can be observed. Locally in the southern part of the massif, slight post-magmatic foliation (N350° to N030° with 50–70°W plunge), associated with a well-developed fracturation, has been observed close to Pan-African faults. Enclaves lengthening (sometimes important, with length/width ratio reaching 10) shows a preferential orientation. Its precise orientation cannot be determined because of outcrop conditions but has a N130° azimuth or is rather close to the N350° slight foliation when the latter exists. The brittle post-magmatic deformation is of variable degree and increases towards the N–S and NNE–SSW faults. The satellite image study agrees with the field observation for the presence of important N–S faults (not indicated on the previous maps), particularly close to the sites 19, 20 and 21 in the southern part of the massif. It also highlights a widespread ENE–WSW fracturation all over the massif. In the site 20, the deformation degree is relatively high with a N345 foliation. An aplitic dyke, clearly affected by brittle deformation, is parallel to this foliation.

3.2. The Arokam-East orthogneiss

On the old geological map, it has been grouped with the Abdou pluton (see below) giving it a particular aspect, with a sub-circular shape in the north (Abdou pluton) and a N–S lengthened shape in its southern part (Arokam-East orthogneiss). Actually, no contact has been found between these two units. This area has been studied in detail through images analysis. Classical image processing have been done like filtering, filtering after Fourrier transform and principal component transformation. A high-pass filtered Fourrier transform has also been merged with a three bands (TM 7, 4 and 2) color composite image to enhance the spectral responses (Fig. 4). The interpretation of this image underlines a

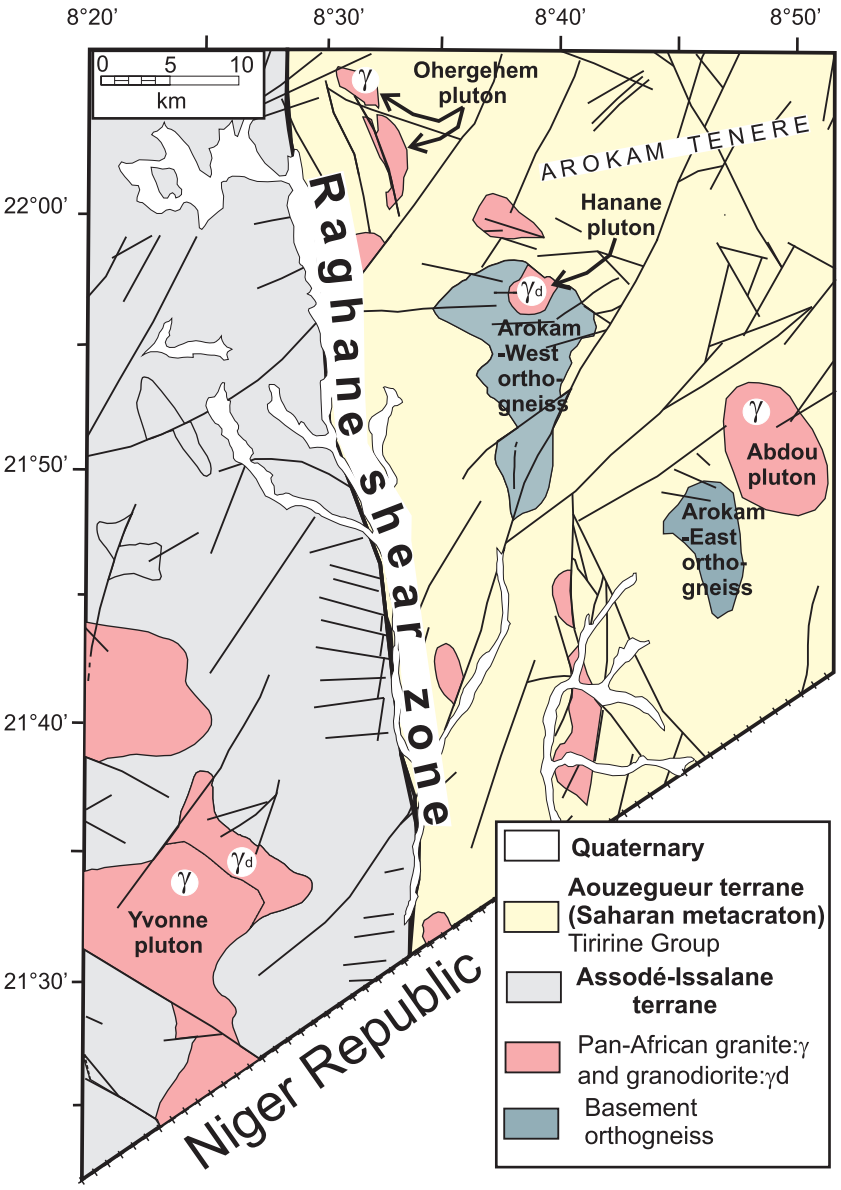

Fig. 2. Geological sketch map of the studied area after Guérangé and Vialon (1960).

N–S boundary between Arokam-East and Abdou. Their textural and spectral responses are very distinct. On the contrary, the surrounding Tiririne Group appears homogeneous with a N–S oriented cleavage all over the studied area.

Arokam-East protolith is very similar to Arokam-West protolith. It is a fine-grained pink biotite granite devoid of amphibole. Other main minerals are quartz, perthitic potassic feldspar and zoned oligoclase (An_{26-29}). Magnetite is the main opaque mineral. Dykes of pink fine-grained granite crosscut Arokam-East and present different directions and plunges (mainly N010° 10°E and N070° vertical).

3.3. The Hanane pluton

The Hanane pluton intruded the Arokam-West orthogneiss in the middle of its northern outcropping part and is constituted of a granodiorite with abundant enclaves. Its primary main minerals are quartz, perthitic orthose, plagioclase (An_{20-28}), biotite, abundant amphibole (edenite and ferro-edenite type), sphene and opaque minerals (mostly magnetite). Fresh biotite has high XFe ratio (0.51) and belongs to the calc-alkaline and sub-alkaline families. In most places, the main minerals do not show visible preferential orientation. Localized magmatic orientation and parallel enclave elongation have been observed at the rim of the pluton along the latter. This reflects a strong shearing event along the pluton margins during its emplacement.

3.4. The Abdou pluton

The Abdou pluton is located close to the Arokam-East orthogneiss outcrop. This pluton is composed of pink medium-grained granite and granodiorite. The latter is mainly located in the middle of the massif, suggesting a ring structure but the outcrops did not allow the full demonstration of such a structure. Both facies contain biotite and amphibole as dark minerals and dark enclaves. Locally (site 66), enclaves lengthening is preferentially oriented along a N030° plunging direction. On the western border, some magma mingling (granite and granodiorite to gabbro) has been

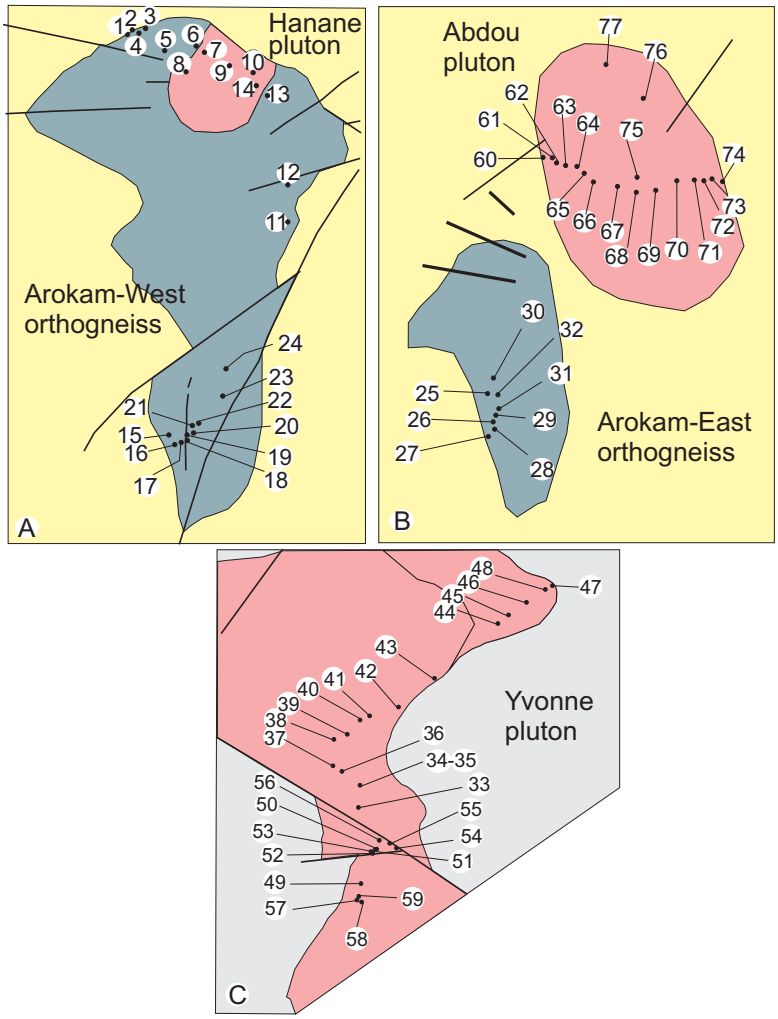

Fig. 3. Sampling sites in the Arokam Ténéré (TI). (A) central plutonic complex; (B) eastern plutonic complex; (C) Yvonne composite pluton.

observed. No deformations have been found around the contacts between the different types of magmatic facies.

3.5. The Yvonne composite pluton

The Yvonne pluton (Black et al., 1967) straddles the Algeria/Niger border. It belongs to the Assodé-Issalane terrane, about 10 km west of the Raghane shear zone. It is indicated as a post-tectonic granite on the existing geological maps. Its largest part is made of a massive fine-grained pink calc-alkaline biotite syenogranite, devoid of amphibole. It can form high reliefs. The northeastern part, separated from the granitic part by a large depression without outcrops, is made of a gray granodiorite with dark enclaves, without preferential orientation of the main minerals. This mesocratic granodiorite bears biotite and amphibole.

The Yvonne granite is crosscut by an important NW–SE fault with associated N090° conjugated faults. This major fault affects the Raghane shear zone in Niger (Black et al., 1967) showing its late character. South of this main fault, an intense fracturation with silicification and fault mirrors is associated with these two fault directions. On Landsat images, the main NW–SE fault appears as a sinistral strike-slip fault. Detailed field observations have not been able to confirm this sense of displacement on the N120° oriented faults. By contrast, the N090° mirrors bear dextral movement markers. No visible foliation or lineation has been observed in the granite or in the granodiorite, but brittle and silicified bands are related to the N090° direction, in alternation with undeformed granitoids.

On satellite images, the Yvonne composite pluton presents three areas, with the granite to the south, the granodiorite to the north-east and between them a complicated area showing both characters of magmatic and host rocks (Fig. 4). That could hide a preserved contact between the two magmatic types. Satellite images displays N040° to N070° orientations within the granite as well as N–S directions. Dykes of pink microgranite crosscut the pluton mainly with N040° and E–W orientations.

4. U–Pb on zircon geochronology

4.1. Analytical techniques

Laser ablation age determinations on zircons from the Arokam Ténéré were performed at the University of Montpellier II (Géosciences Montpellier) on an Element XR sector field ICP-MS coupled to a Lambda Physik Compex 102 excimer laser (193 nm). Analytical procedures followed those outlined in Bruguier et al. (2001) and Neves et al. (2006). Samples were ablated under helium in a 15 cm^3, circular shaped cell using an energy density of 15 J/cm^2 at a frequency of 4 Hz. Laser spot sizes were 26 μm, except for BT2 sample for which few grains with complex internal

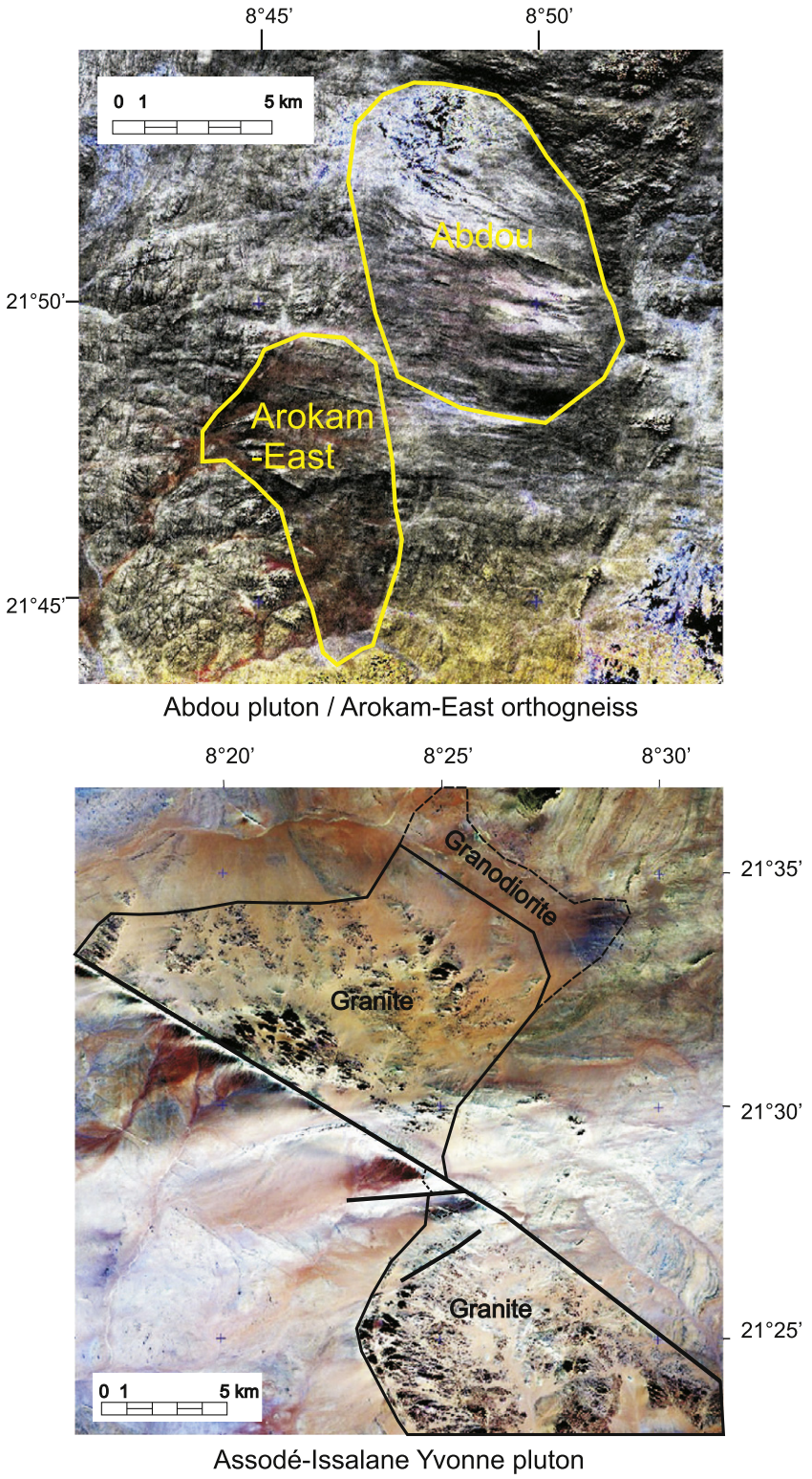

Fig. 4. Interpretation of the eastern and western areas from Landsat processed image, pointing the presence of different plutons in north and in south of the massifs. (Free data from GLCF/University of Maryland.)

structures were analyzed using 15 μm spot size (analyses labeled ∗ in Table 1). The well characterized zircon standard G91500 (Wiedenbeck et al., 1995) was used to correct the collected data for mass discrimination and inter-element fractionation and has been analyzed 44 times in the course of this study (three sessions). Before analyses, the instrument was tuned in order to give stable signals and the maximum sensitivity for ^{206}Pb and ^{238}U, while keeping low oxide production rates (generally 1% and below for ThO^+/Th^+, and 0.5% for UO^+/U^+). Measured masses are ^{202}Hg, ^{204}(Pb^+Hg), ^{206}Pb, ^{207}Pb, ^{208}Pb, ^{232}Th and ^{238}U using fifteen points per peak and a 20% mass window resulting in three measured points for each mass station. All isotopes were measured during 10.24 ms except ^{207}Pb which was measured during 40.96 ms and ^{202}Hg and ^{204}(Hg^+Pb) which were measured during 5.12 ms. Total

Table 1
La-ICP-MS U–Pb data on zircon for Arokam-West orthogneiss, Hanane, Abdou and Yvonne plutons. Analyses labeled * correspond to 15 μm spot diameter of the laser beam. All other analyses have been performed using a 26 μm spot size.

Spot name	ppm U	ppm Th	Th/U	ppm Pb*	$^{207}Pbr/^{206}Pbr$	1σ abs	$^{207}Pbr/^{235}U$	1σ abs	$^{206}Pbr/^{238}U$	1σ abs	Err corr	$^{207}Pb/^{206}Pb$ age	1σ abs	$^{206}Pb/^{238}U$	1σ abs	%Disc
BT2-Arokam orthogneiss																
#1-	75	42	0.56	28.4	0.1168	0.0006	5.4645	0.0759	0.3395	0.0044	0.93	1907	9	1884	21	98.8
#2-1 core	924	516	0.56	358	0.1180	0.0005	5.6736	0.0693	0.3488	0.0040	0.95	1926	7	1929	19	100.1
#2-2 rim*	1218	99	0.08	163	0.0830	0.0009	1.5264	0.0303	0.1334	0.0022	0.83	1269	22	807	12	63.6
#2-3 core*	792	406	0.51	311	0.1187	0.0007	5.8263	0.0607	0.3560	0.0030	0.80	1937	11	1963	14	101.4
#2-4 rim*	1249	16	0.01	120	0.0670	0.0005	0.9337	0.0088	0.1011	0.0006	0.65	838	15	621	4	74.1
#2-5 rim*	1004	112	0.11	179	0.0965	0.0009	2.3062	0.0306	0.1732	0.0017	0.72	1558	17	1030	9	66.1
#3-1	604	221	0.37	224	0.1171	0.0005	5.6507	0.0589	0.3499	0.0034	0.92	1913	7	1934	16	101.1
#4-1	70	40	0.57	25.7	0.1170	0.0006	5.3913	0.0671	0.3341	0.0038	0.91	1911	9	1858	18	97.2
#4-2	783	392	0.50	304	0.1178	0.0005	5.7358	0.0633	0.3532	0.0036	0.93	1923	7	1950	17	101.4
#5-1	156	101	0.65	55.2	0.1166	0.0005	5.0889	0.0685	0.3166	0.0040	0.94	1904	8	1773	20	93.1
#6-1 ext core	116	87	0.75	45.8	0.1180	0.0005	5.7300	0.0420	0.3520	0.0021	0.81	1927	8	1944	10	100.9
#6-2 core	860	498	0.58	340	0.1179	0.0004	5.7103	0.0507	0.3513	0.0029	0.92	1924	6	1941	14	100.9
#6-3 ext core*	159	92	0.58	59.9	0.1179	0.0008	5.4299	0.0701	0.3340	0.0036	0.83	1925	13	1858	17	96.5
#6-4 core*	261	232	0.89	108	0.1175	0.0007	5.6268	0.0523	0.3474	0.0025	0.78	1918	10	1922	12	100.2
#7-1	280	261	0.93	119	0.1176	0.0005	5.6755	0.0388	0.3501	0.0019	0.81	1920	7	1935	9	100.8
#7-2 rim*	1011	114	0.11	197	0.0973	0.0006	2.6192	0.0379	0.1952	0.0026	0.91	1574	11	1149	14	73.0
#8-1	319	233	0.73	125	0.1170	0.0004	5.4439	0.0515	0.3376	0.0030	0.93	1910	6	1875	14	98.1
#9-1	297	212	0.71	119	0.1175	0.0004	5.6306	0.0718	0.3475	0.0042	0.96	1919	7	1923	20	100.2
#10-1	768	436	0.57	306	0.1180	0.0004	5.7101	0.0477	0.3510	0.0027	0.91	1926	6	1939	13	100.7
#11-1	114	61	0.54	42.3	0.1175	0.0005	5.4549	0.0409	0.3368	0.0020	0.81	1918	8	1871	10	97.6
#12-1	189	116	0.61	75.3	0.1173	0.0005	5.4739	0.0940	0.3384	0.0057	0.97	1916	7	1879	27	98.1
#13-1	454	228	0.50	176	0.1169	0.0004	5.6490	0.0422	0.3503	0.0023	0.88	1910	6	1936	11	101.4
#14-1	755	504	0.67	312	0.1177	0.0004	5.7147	0.0462	0.3522	0.0026	0.90	1921	6	1945	12	101.2
#14-2	596	329	0.55	240	0.1177	0.0004	5.7917	0.0456	0.3570	0.0025	0.90	1921	6	1968	12	102.4
#15-1*	1800	1296	0.72	780	0.1182	0.0007	5.9630	0.0502	0.3660	0.0023	0.76	1929	10	2011	11	104.2
#16-1*	920	419	0.46	360	0.1176	0.0006	5.8327	0.0613	0.3597	0.0032	0.85	1920	10	1981	15	103.1
#17-1*	822	551	0.67	339	0.1183	0.0007	5.8342	0.0530	0.3578	0.0025	0.78	1930	10	1972	12	102.2
#18-1*	776	312	0.40	220	0.1095	0.0007	3.9025	0.1151	0.2585	0.0074	0.98	1791	12	1482	38	82.8
#19-1*	1166	505	0.43	452	0.1171	0.0006	5.8014	0.0494	0.3592	0.0023	0.77	1913	10	1978	11	103.4
BT3-Hanane pluton																
#1-1	145	97	0.67	16.3	0.0627	0.0003	0.9083	0.0083	0.1051	0.0008	0.81	697	11	644	5	92.5
#2-1	139	99	0.71	16.0	0.0609	0.0003	0.8964	0.0125	0.1068	0.0014	0.93	634	11	654	8	103.1
#3-1	180	134	0.75	21.1	0.0622	0.0003	0.9325	0.0097	0.1087	0.0010	0.88	681	10	665	6	97.7
#4-1	159	64	0.40	14.6	0.0596	0.0003	0.7683	0.0095	0.0935	0.0011	0.92	589	10	576	6	97.9
#4-2	58	24	0.41	5.4	0.0593	0.0004	0.7628	0.0093	0.0933	0.0009	0.82	578	15	575	6	99.5
#5-1	61	46	0.76	8.1	0.0630	0.0007	1.0604	0.0143	0.1220	0.0010	0.59	710	23	742	6	104.6
#6-1	20	17	0.81	2.7	0.1161	0.0016	1.6406	0.0264	0.1025	0.0008	0.48	1897	25	629	5	33.2
#7-1	188	143	0.76	22.6	0.0611	0.0004	0.9154	0.0105	0.1087	0.0010	0.81	642	14	665	6	103.6
#8-1	266	175	0.66	31.8	0.0665	0.0005	1.0056	0.0114	0.1097	0.0010	0.79	821	14	671	6	81.7
#8-2	282	160	0.57	29.7	0.0593	0.0005	0.7739	0.0101	0.0946	0.0010	0.79	579	17	583	6	100.6
#9-1	117	84	0.72	13.4	0.0613	0.0005	0.8826	0.0188	0.1044	0.0021	0.93	651	17	640	12	98.3
#10-1	431	240	0.56	51.7	0.0623	0.0004	0.9633	0.0162	0.1122	0.0017	0.92	683	14	686	10	100.3
#11-1	849	726	0.85	161	0.0625	0.0004	0.9183	0.0179	0.1066	0.0020	0.95	691	12	653	12	94.5
#12-1	118	45	0.38	13.0	0.0612	0.0005	0.9035	0.0174	0.1072	0.0019	0.90	645	18	656	11	101.8
#13-1	63	25	0.40	6.4	0.0592	0.0006	0.7759	0.0107	0.0951	0.0009	0.68	573	22	586	5	102.3
#14-1	138	52	0.38	13.0	0.0595	0.0005	0.7668	0.0084	0.0934	0.0007	0.65	587	18	576	4	98.1
#15-1	139	103	0.74	17.0	0.0633	0.0006	0.9432	0.0128	0.1080	0.0010	0.70	720	20	661	6	91.8
#15-2	131	64	0.49	14.6	0.0638	0.0005	0.9380	0.0106	0.1066	0.0008	0.70	735	17	653	5	88.9
#16-1	784	585	0.75	106	0.0679	0.0005	0.9593	0.0139	0.1025	0.0012	0.84	865	16	629	7	72.7
#17-1	600	297	0.50	70.7	0.0649	0.0004	0.9880	0.0103	0.1103	0.0010	0.84	772	12	675	6	87.3
#18-1	77	28	0.36	7.4	0.0585	0.0007	0.7648	0.0111	0.0948	0.0008	0.62	549	25	584	5	106.4
#18-2	64	27	0.42	6.3	0.0594	0.0007	0.7803	0.0109	0.0952	0.0007	0.56	584	25	586	4	100.5
#19-1	128	85	0.66	15.6	0.0611	0.0004	0.9346	0.0119	0.1110	0.0012	0.84	641	15	679	7	105.8
#20-1	324	138	0.43	30.9	0.0599	0.0009	0.7847	0.0128	0.0949	0.0007	0.46	602	31	585	4	97.2
BT8-Yvonne pluton																
#1-1	469	52	0.11	45.5	0.0600	0.0003	0.8414	0.0102	0.1017	0.0011	0.89	604	12	624	6	103.3
#2-1	761	20	0.03	73.7	0.0612	0.0004	0.8717	0.0089	0.1033	0.0008	0.75	647	14	634	5	98.0
#3-1	972	65	0.07	91.2	0.0602	0.0012	0.8417	0.0173	0.1014	0.0004	0.20	611	43	623	2	101.9
#4-1	1178	31	0.03	138	0.0611	0.0004	0.8920	0.0073	0.1059	0.0005	0.61	643	14	649	3	101.0
#5-1	78	55	0.70	29.6	0.1180	0.0008	5.4365	0.0780	0.3341	0.0042	0.87	1926	13	1858	20	96.5
#6-1	253	29	0.11	25.0	0.0614	0.0004	0.8819	0.0093	0.1041	0.0009	0.84	655	12	638	5	97.5
#6-2	164	37	0.22	27.8	0.0902	0.0025	2.1661	0.1103	0.1741	0.0075	0.84	1430	51	1035	41	72.3
#7-1	93	82	0.87	37.0	0.1167	0.0012	5.2269	0.0828	0.3247	0.0040	0.78	1907	18	1813	19	95.1
#8-1	1402	89	0.06	141	0.0621	0.0003	0.8926	0.0080	0.1043	0.0007	0.80	677	11	639	4	94.4
#9-1	162	43	0.26	31.7	0.0965	0.0005	2.4713	0.0268	0.1856	0.0018	0.88	1558	10	1098	10	70.4
#10-1	249	24	0.10	23.2	0.0595	0.0004	0.7960	0.0092	0.0970	0.0010	0.85	586	13	597	6	101.8
#11-1	1447	50	0.03	138	0.0605	0.0003	0.8438	0.0056	0.1011	0.0005	0.75	622	9	621	3	99.8
#12-1	45	54	1.20	6.2	0.0615	0.0007	0.9174	0.0137	0.1082	0.0009	0.58	657	26	662	5	100.8

(*continued on next page*)

Table 1 (*continued*)

Spot name	ppm U	ppm Th	Th/U	ppm Pb*	$^{207}Pbr/^{206}Pbr$	1σ abs	$^{207}Pbr/^{235}U$	1σ abs	$^{206}Pbr/^{238}U$	1σ abs	Err corr	$^{207}Pb/^{206}Pb$ age	1σ abs	$^{206}Pb/^{238}U$	1σ abs	%Disc
#13-1	2427	52	0.02	215	0.0603	0.0002	0.8036	0.0092	0.0967	0.0011	0.96	614	7	595	6	96.9
#13-2	2573	68	0.03	234	0.0599	0.0003	0.8006	0.0087	0.0969	0.0009	0.89	602	11	596	6	99.1
#14-1	2043	90	0.04	180	0.0598	0.0003	0.7942	0.0072	0.0963	0.0007	0.85	596	10	593	4	99.4
#15-1	1958	92	0.05	176	0.0599	0.0003	0.7999	0.0083	0.0968	0.0009	0.91	602	9	595	5	99.0
#15-2	2313	94	0.04	202	0.0600	0.0002	0.7891	0.0118	0.0954	0.0014	0.96	603	9	587	8	97.4
#16-1	1583	53	0.03	143	0.0603	0.0003	0.8070	0.0104	0.0970	0.0012	0.92	616	11	597	7	96.9
#17-1	1909	76	0.04	171	0.0600	0.0002	0.7925	0.0113	0.0958	0.0013	0.96	603	9	590	8	97.9
#17-2	2681	119	0.04	232	0.0598	0.0003	0.7934	0.0149	0.0962	0.0018	0.97	597	10	592	10	99.1
#18-1	1464	94	0.06	132	0.0600	0.0003	0.7955	0.0110	0.0962	0.0013	0.95	603	9	592	7	98.2
#18-2	1013	64	0.06	91.1	0.0598	0.0002	0.7930	0.0124	0.0961	0.0015	0.97	598	8	592	9	98.9
#19-1	1504	41	0.03	131	0.0596	0.0002	0.7917	0.0064	0.0963	0.0007	0.89	590	8	593	4	100.4

acquisition time was 60 s with the first 15 s devoted to gas blank measurement. ^{202}Hg was used to monitor the ^{204}Hg interference on ^{204}Pb, but common Pb correction were not performed as this often resulted in over-correction, the 204 mass being largely dominated by ^{204}Hg. Data presented in this study thus only report analyses for which no common Pb was detected.

Raw data were exported from the ICP-MS and processed off-line with an Excel spreadsheet. Measured intensities were grouped by batches integrating *c.* 1 s of measurements and were subsequently background corrected. Calculated isotopic ratios were then corrected for instrumental mass discrimination (Pb/Pb ratios) and inter-element, laser induced, fractionation ($^{206}Pb/^{238}U$ ratios) by normalization to the G91500 zircon standard. For mass bias correction all standards measured during one analytical session were used to calculate a mass bias factor (power law). Following Horstwood et al. (2003), uncertainty reported for the $^{207}Pb/^{206}Pb$ ratio of each unknown corresponds to the quadratic addition of the external reproducibility obtained from the measurements of the G91500 zircon standard and the within-run precision of each individual analysis. Variations in the $^{206}Pb/^{238}U$ ratio are much more sensitive to analytical conditions, and in order to minimize drift, the Pb/U ratios of unknowns were calibrated against the inter-element bias factor calculated from four measurements of the G91500 zircon standard bracketing a group of five unknowns. Similarly to the $^{207}Pb/^{206}Pb$ ratios, errors quoted for the $^{206}Pb/^{238}U$ ratios correspond to the quadratic addition of the external reproducibility obtained from the measurements of the four G91500 standards and the within-run precision of each analysis. Since the ^{235}U isotope was not measured, the quoted $^{207}Pb/^{235}U$ ratios were derived from the corrected $^{207}Pb/^{206}Pb$ and $^{206}Pb/^{238}U$ ratios assuming a $^{238}U/^{235}U$ ratio of 137.88. Reported uncertainties on this ratio were derived from the quadratic addition of the uncertainties of the $^{207}Pb/^{206}Pb$ and $^{206}Pb/^{238}U$ ratios. Ages were calculated using the IsoplotEx program of Ludwig (2003). Data are given in Table 1.

4.2. Results

Twenty-nine spots have been performed on zircons from sample BT2, representing the *Arokam-West orthogneiss*. The zircon crystals display large cores with euhedral to subeuhedral shapes with oscillatory zoning concordant with the external shape, rarely discordant. Rims of variable thickness can be seen around these cores or transgressive on the cores (Fig. 5), but are often too thin to be dated. However four spots (15 μm) have been done on the largest ones. The remaining 25 spots concern the central parts of the zircon crystals.

All the 29 spots define a discordia line (MSWD = 1.6) giving a well-defined upper intercept of 1918 ± 5 Ma and a lower intercept of 580 ± 26 Ma (Fig. 5). 23 central domains are located close to the upper intercept and the age of 1918 ± 5 Ma can be interpreted as the age of crystallization of the Arokam-West protolith. The four rims analyzed are strongly discordant, one of them (#2–3 rim) being close to the lower intercept at *c.* 580 Ma. All rims have low Th/U ratios (from 0.01 to 0.11) which contrast with the Th/U ratio of the central domains (from 0.40 to 0.89). The age of 580 ± 26 Ma is thus interpreted as the age of the Arokam-West gneissification. The fact that the rim spots are not concordant at *c.* 580 Ma is most likely due to the volume analyzed by the laser, which had to be

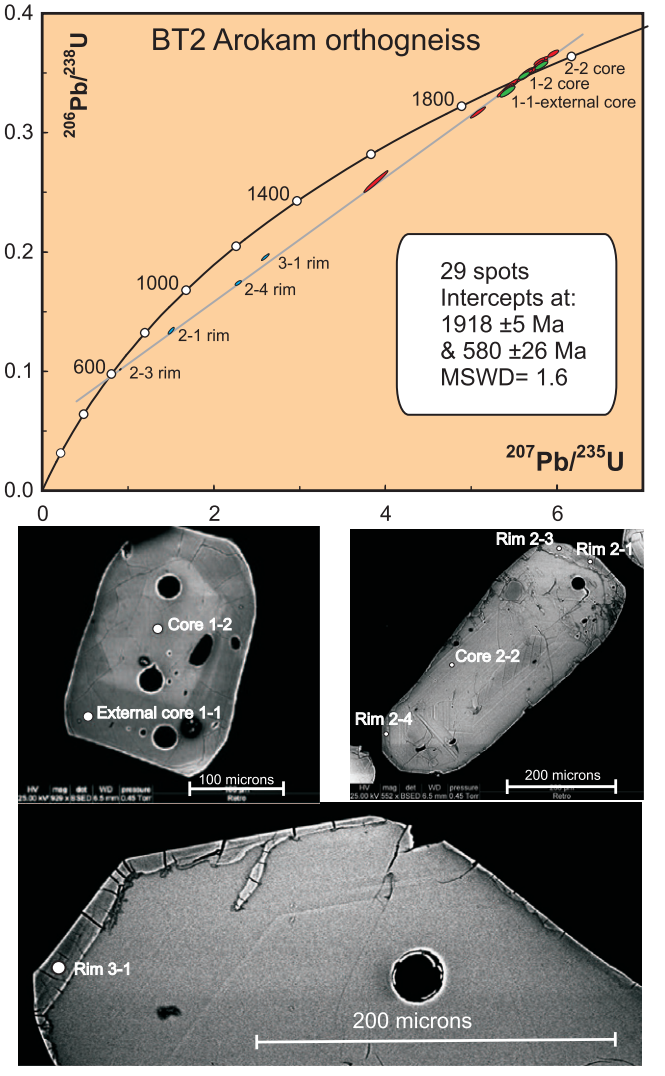

Fig. 5. Concordia diagram for BT2 (Arokam-West orthogneiss) zircons and backscattered SEM images of three crystals showing the thin Pan-African rims around Eburnean cores.

inevitably a mixing between the rims and the cores, if considering the thinness of the rims or to partial recrystallization. It can be concluded that the Arokam-West pluton crystallized at 1918 ± 5 Ma and was affected by an event that allowed the slight recrystallization of zircons at 580 ± 26 Ma. The thinness of the zircon rims is in agreement with the faint gneissic structure of the Arokam-West orthogneiss.

Twenty-four spots have been performed on zircons from sample BT3, representing the *Hanane pluton*. Eight spots are concordant and define an age of 582 ± 3 Ma that can be interpreted as the age of crystallization of the Hanane pluton (Fig. 6A). This age is, within error limits, identical to the lower intercept given by the Arokam-West orthogneiss. Numerous zircons (16 spots) are xenocrystic. Their ages span from 640 to 680 Ma, with an age at *c.* 730 Ma, corresponding to the Neoproterozoic oceanic thrust nappes known in the Aouzegueur terrane (Caby and Andreopoulos-Renaud, 1987; Liégeois et al., 1994). No Eburnean zircons have been found.

Twenty-four spots have been performed on zircons from sample BT8, representing the *Yvonne granite*. Ten spots are concordant and define an age of 595 ± 3 Ma that can be interpreted as the age of crystallization of the Yvonne granite (Fig. 6B). This age is older than that of the Hanane pluton, but identical to the age of the Ohergehem pluton (Fig. 2; 594 ± 4 Ma; Henry et al., 2009) and to the Dabaga-East plutons in Aïr, characteristic of the Assodé-Issalane terrane. As for the Hanane pluton, numerous zircons (14 spots) are xenocrystic. Their ages span from 620 to 660 Ma corresponding to the age of the early Dabaga-East batholiths (Liégeois et al., 1994). No Eburnean zircons have been found.

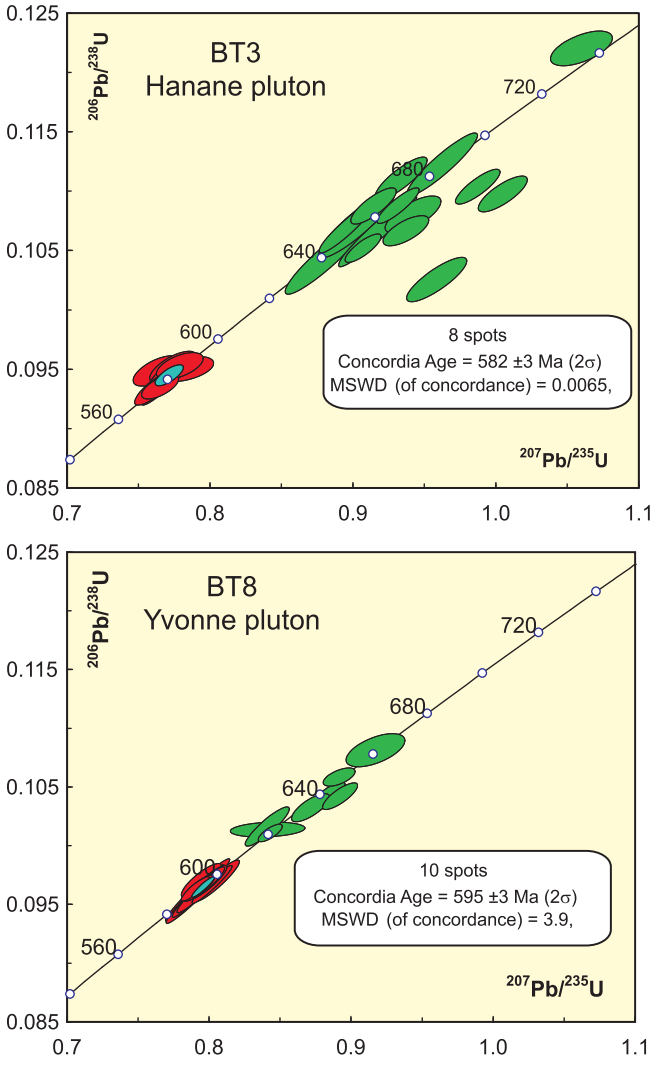

Fig. 6. Concordia diagram for BT3 (Hanane pluton) zircons and BT8 (Yvonne pluton) zircons.

5. Geochemical and Sr–Nd isotopic compositions

Representative samples of the studied units, including the samples dated by the U–Pb method, have been analyzed for major and trace elements (Table 2) and for Sr and Nd isotopic composition (Table 3). Major elements were determined by ICP-AES and trace elements by ICP-MS in the Geochemical Laboratory of the Royal Museum for Central Africa in Tervuren (see Liégeois et al., 2003 for analytical procedures). Sr and Nd isotopes: after acid dissolution of the sample and Sr and/or Nd separation on ion-exchange resin, Sr isotopic compositions have been measured on Ta simple filament and Nd isotopic compositions on triple Ta–Re–Ta filament in a TIMS (thermal ionization mass spectrometer) VG Sector 54 from the Isotope Geology division of the Royal Museum for Central Africa, Tervuren. Repeated measurements of Sr and Nd standards have shown that between-run error is better than 0.000015 (2σ). During the course of this study, the NBS987 standard yields values for $^{87}Sr/^{86}Sr$ between 0.710278 ± 0.000006 and 0.710290 ± 0.000007 (2σ on the mean of the four standards measured for each set of 16 samples, normalized to $^{86}Sr/^{88}Sr = 0.1194$) and the Rennes Nd standard values for $^{143}Nd/^{144}Nd$ between 0.511950 ± 0.000007 and 0.511961 ± 0.000009 (2σ on the mean of the four standards measured for each set of 16 samples, normalized to $^{146}Nd/^{144}Nd = 0.7219$. All measured ratios have been normalized to the recommended values of 0.710250 for NBS987 and 0.511963 for Nd Rennes standard (corresponding to a La Jolla value of 0.511866). The Rb–Sr and Sm–Nd ages have been calculated following Ludwig (2003). Decay constant for ^{87}Rb (1.42×10^{-11} a^{-1}) was taken from Steiger and Jäger (1977) and for ^{147}Sm (6.54×10^{-12} a^{-1}) from Lugmair and Marti (1978).

The Arokam orthogneiss is granitic in composition and close to the calc-alkalic/alkali-calcic boundary (Fig. 7A). Abdou and Hanane analyzed samples are granodioritic and belong to the calc-alkalic series while the Yvonne pluton, from the Assodé-Issalane pluton, belongs to the alkali-calcic series (Fig. 7A). Rare Earth elements (Fig. 7B) and incompatible elements as a whole (Fig. 7C) show that the Arokam-West orthogneiss (*c.* 1.92 Ga), Abdou (*c.* 595 Ma) and Hanane (*c.* 582 Ma) plutons have close compositions corresponding to a calc-alkaline composition. Hanane pluton is less enriched in several LILE (Large Ion Lithophile Elements), namely K, Rb, Th and in Nb–Ta (Fig. 7C). The Yvonne granodiorite, in agreement with its alkali-calcic nature, is enriched in REE and presents a higher LREE/HREE fractionation and as a whole enriched in HFSE (High Field Strength Elements, from Nb to Yb in Fig. 7C). The Yvonne granite has been affected by subsolidus element mobility, probably with the interaction of F- and Cl-rich fluids, able to generate seagull-like spectra (tetrad effect, enrichment in HREE; Bau, 1996; Veksler et al., 2005). The positive Ce anomaly could be due to the poor solubility of Ce^{4+} compared to other trivalent REE in an oxidizing alkaline environment. This Ce abundance is probably close to the initial magmatic concentration. This fluid-rich event could be linked to the main fault that cut the Yvonne pluton in two parts.

The Sr and Nd isotopic ratios have been recalculated at the zircon age of each massif. The age of Abdou is not known but it can be considered to be between 595 and 580 Ma and has been set to that of Hanane, at *c.* 582 Ma. In Fig. 8, the initial ratios of the studied rocks have been reported together with regional references: Dabaga-East (Liégeois et al., 1994) are granitoids in Aïr to the south, east of the Raghane shear zone; Dabaga-West and Renatt (Liégeois et al., 1994) are granitoids in Aïr to the south, west of the Raghane shear

Table 2
Whole rock geochemistry (major and trace elements) for Arokam-West orthogneiss, Hanane, Abdou and Yvonne plutons. Ages are U–Pb zircon ages (LA-ICP-MS, this study) except those in brackets that are inferred ages.

Unit	Age	Site	Name	SiO_2	Al_2O_3	Fe_2O_{3t}	MnO	MgO	CaO	Na_2O	K_2O	TiO_2	P_2O_5	PF	Total
Arokam-W	1915	Site 5	BT2	68.24	16.25	3.25	0.06	0.73	2.47	4.85	3.60	0.42	0.14	0.75	100.77
Arokam-E	(1915)	Site 25	BT7A	71.11	14.96	2.55	0.06	0.71	1.89	3.98	4.15	0.35	0.14	0.59	100.49
Abdou	(<582)	Site 72	BT7B	63.68	16.43	5.01	0.09	1.44	3.75	4.66	1.99	0.53	0.20	1.05	98.86
Hanane	582		BT3	61.18	16.06	5.53	0.08	3.56	5.02	3.91	2.90	0.64	0.24	0.68	99.79
Yvonne Gr	594		BT8	77.03	12.84	1.10	0.03	0.11	0.41	3.24	5.77	0.07	0.01	0.21	100.81
Yvonne Gd	(>594)	Site 45	BT8B	64.15	15.85	4.83	0.07	1.64	3.37	4.06	3.61	0.60	0.18	0.79	99.15

Name	Sr	Ba	V	Rb	Y	Zr	Nb	La	Ce	Pr	Nd	Sm	Eu	Gd	Dy	Ho
BT2	312	1364	26	80	29.6	322	11.8	24.8	63.2	7.29	28.9	5.85	1.28	5.51	5.01	0.96
BT7A	301	846	25	151	13.4	169	17.7	26.1	60.5	5.40	18.8	3.22	0.71	2.95	2.14	0.40
BT7B	417	1068	63	45	23.8	342	6.5	17.8	44.6	4.51	18.7	3.97	1.13	3.98	3.81	0.76
BT3	578	849	96	97	17.6	224	8.7	33.3	72.7	7.61	28.1	4.96	1.17	4.28	3.09	0.57
BT8	29	53	7	260	50.0	40	22.3	1.83	22.7	0.91	4.79	2.56	0.26	3.88	6.45	1.39
BT8B	335	894	58	125	35.0	497	18.4	87.6	170.6	16.9	55.6	8.36	1.49	7.40	5.76	1.13

	Er	Yb	Lu	Hf	Ta	W	Pb	Th	U	Co	Cu	Ga	Ge	Ni	Sc	Zn
BT2	2.87	2.71	0.39	7.20	0.77	3.27	9.9	7.07	1.93	6.42	12.6	19.8	1.4	1.9	9.1	42
BT7A	1.22	1.30	0.20	4.25	1.63	4.32	22.0	15.9	6.50	8.04	12.1	17.6	1.4	5.1	6.5	40
BT7B	2.32	2.15	0.32	7.40	0.23	7.37	11.8	3.10	1.06	9.80	17.7	18.3	1.2	10.9	12.4	65
BT3	1.64	1.52	0.22	5.09	0.56	3.36	20.3	14.5	2.69	66.9	37.1	19.2	1.2	75.5	13.5	61
BT8	4.68	5.11	0.77	2.13	2.20	8.29	36.1	10.2	5.93	0.96	12.2	19.5	1.9	4.2	6.0	43
BT8B	3.45	3.38	0.51	10.7	1.06	4.04	23.3	25.1	2.34	96.8	17.2	23.2	1.3	59.3	11.5	65

zone and Ounane (Liégeois et al., 2003) is a large granodioritic pluton located to the north, west of the Raghane shear zone. It shows that Arokam orthogneiss and Abdou pluton lies within the field of the granitoids characteristic of the Saharan metacraton, to the east of the Raghane shear zone. Having a similar signature for *c.* 1.92 Ga and *c.* 0.58 Ga granitoids suggest the reactivation of the Eburnean source in the Pan-African times, in agreement with the metacraton concept (Liégeois et al., 2003; De Waele et al., 2006). TDM model age of Arokam orthogneiss is around 1.6 Ga, a little younger than the zircon age (1.92 Ga). This can be attributed either to the model used for calculating these model ages (Nelson and DePaolo, 1985), that of Goldstein et al. (1984) for example giving typically 100–200 m.y. older values (see complete discussion in Liégeois and Stern, 2010). Whatever, this Nd model ages indicates that the protolith of the Arokam orthogneiss was a Paleoproterozoic juvenile magma. The slightly younger model age of Abdou (*c.* 1.45 Ga) suggests the addition a mantle component, probably at the origin of the partial melting of the Eburnean lithospheric source.

The Hanane pluton is located between the Arokam and the depleted mantle signatures, suggesting the involvement of a greater mantle component than for Abdou. This can be correlated with its lower concentration in HFSE (Fig. 7C).

By contrast, the Yvonne pluton present much lower ε_{nd} values (−17.5 and −19.5) and higher initial $^{87}Sr/^{86}Sr$ (*c.* 0.711). This is in agreement with the global Sr–Nd signature of the Assodé-Issalane terrane (Liégeois et al., 1994) and the Ounane region (Liégeois et al., 2003), west of the Raghane shear zone (Fig. 8). There, the geodynamical situation is different as a regional partial melting occurred that attained the Rb-undepleted medium crust (Liégeois et al., 1994). The Yvonne granite sample has actually $a < 0.7$ Sr initial ratio, which can be linked to the subsolidus fluid-enriched episode.

6. Rock magnetism and AMS studies

6.1. Sampling

More than 550 oriented cores have sampled in 77 sites in the three studied areas (Arokam-West and Hanane area, Fig. 3A; Arokam-East and Abdou area, Fig. 3B; Yvonne area, Fig. 3C), mainly along cross-sections perpendicular to the main faults affecting them, for AMS and rock magnetism studies. Most of them correspond to granitic or granite–gneissic facies. For the Arokam-West orthogneiss, two cross-sections with sampling have been done in the northern (nine sites, 64 core-samples) and southern (10 sites, 79 core-samples) part of the massif. For the Hanane granodiorite, 37 core-samples have been collected in five sites. For the eastern area, two cross-sections have been studied in the Abdou granitoid pluton (18 sites, 131 core-samples) and Arokam-East orthogneiss (10 sites, 65 core-samples). Two NNE–SSW cross-sections in the Yvonne granitoids pluton have been sampled, in the northern side (12 sites, 74 core-samples in the granite and five sites with 31 core-samples in the granodiorite) and in the southern side (10 sites, 75 core-samples in the granite) of the WNW–ESE major fault that divides the pluton in two parts. In the three areas, core-samples have been also taken from late-magmatic dykes crossing the main intrusions.

6.2. Rock magnetism

The rock magnetism and magnetic fabric measurements were performed at the paleomagnetism laboratory of the IPGP in Saint-Maur. The mean susceptibility in low field km has been measured using a KLY3 Kappabridge.

- It is relatively high. In the Arokam-West/Hanane area, it has values between 1400 and 30,000 $\times 10^{-6}$ SI (Fig. 9) except for some sites where the susceptibility values are much lower (e. g. sites 19, 20 corresponding to highly fractured rocks). The mean susceptibility appears in average to be higher in the granodiorites than in the granites and orthogneiss, though the highest values correspond to sites with coarse orthogneiss.
- In the Abdou pluton, the highest km value of 30,233 $\times 10^{-6}$ SI has been obtained in a granitic site (73), but other sites in the granites also have high km values (sites 74 and 75); in the granodioritic sites, mean susceptibility is also quite high (6272–17,910). The km values in Arokam-East orthogneiss are lower, with 9324 as the highest value.
- In the Yvonne pluton, the highest values are related to the granodiorite (sites 44–48 – larger than 18,000 $\times 10^{-6}$ SI), while it does not exceed 4190 $\times 10^{-6}$ SI in the granite.

Table 3
Rb–Sr and Sm–Nd isotopic compositions on whole rock for Arokam-West orthogneiss, Hanane, Abdou and Yvonne plutons. Ages are U–Pb zircon ages (LA-ICP-MS, this study) except those in brackets that are inferred ages.

Unit	Age		Rb	Sr	$^{87}Rb/^{86}Sr$	$^{87}Sr/^{86}Sr$	2σ	Sri 582 Ma	Sri 595 Ma	Sm	Nd	$^{147}Sm/^{144}Nd$	$^{143}Nd/^{144}Nd$	2σ	ε_{Nd} 582 Ma	ε_{Nd} 595 Ma	T_{DM}
Arokam-West	1915	Site 5	BT2	80.4	312	0.7458	0.712105	0.000009	0.705916	0.705777	5.85	28.89	0.122399	0.512069	0.000009	−5.58	−5.46	1622
Arokam-East		Site 25	BT7A	151.5	301	1.4592	0.716230	0.000008	0.704120	0.703849	3.22	18.77	0.103754	0.511897	0.000007	−7.55	−7.40	1585
Abdou		Site 72	BT7B	97.3	578	0.4876	0.708848	0.000008	0.704801	0.704711	4.96	28.06	0.106882	0.512026	0.000008	−5.26	−5.11	1448
Hanane	582		BT3	45.5	417	0.3150	0.706275	0.000010	0.703661	0.703602	3.97	18.69	0.128374	0.512500	0.000009	2.39	2.51	974
Yvonne Gr	594		BT8	260.2	28.6	26.8440	0.916910	0.000017	0.694141	0.710000	2.56	4.79	0.322847	0.512136	0.000010	−19.20	−19.42	–
Yvonne Gd		Site 45	BT8B	124.7	335	1.0800	0.720492	0.000010	0.711529	0.711328	8.36	55.63	0.090828	0.511329	0.000007	−17.68	−17.51	2128

– In the sampled aplitic dykes, the mean susceptibility is quite low (<900×10^{-6} SI) except for three sites (60a, 67a and 72a) sampled in Abdou pluton with values between 1496 and 8250×10^{-6} SI. However, even within these sites, the susceptibility values in dykes remain lower than the susceptibility of geographically associated granite or granodiorite.

The $K(T)$ curves (mean susceptibility in low field as a function of the temperature) have been determined with a Kappabridge KLY-3 associated with a CS2-3 equipment. Typical curves (Fig. 10) show that magnetite is present in all the studied rocks. In the magnetite-rich samples, presence of minor amount of other magnetic phases could be hidden by this strongly dominant phase.

– In the Hanane, Arokam-West and -East granitoids and dykes, the $K(T)$ curve is generally similar, indicating only the presence of large grains of pure magnetite as shown by its rectangular shape, the absence of well-expressed Hopkinson peak (O'Reilly, 1984) and the sharp decrease of the susceptibility value around 580 °C. Mostly, only a very weak mineralogical alteration (occurrence of a very low amount of newly-formed magnetite) affected the rock during heating around 550–600 °C (samples TR009, TR056 and TR238 on Fig. 10). That is not the case in the granite and aplitic dykes from highly fractured area where this mineralogical alteration is more important and where the presence of other mineralogical phases is evidenced (sample TR129 on Fig. 10). One of these phases has Curie temperature T_c lower than magnetite (around 500 °C) and partly results also from the mineralogical alteration. The other phase on the contrary has Curie temperature higher than 580 °C and is of the hematite family.
– Some differences appear in the Abdou pluton. Here both granite and aplitic dykes show evidence of several components, always dominated by the magnetite phase. Abdou granite (sample TR452 on Fig. 10) presents two dominant components, pure magnetite with T_c of 580 °C and the other one with T_c around 535 °C (titanomagnetite or titanohematite ?).
– For the Yvonne granodiorite, only large grains of pure magnetite clearly can be inferred from $K(T)$ curves (sample TR349 on Fig. 10). Another component with lower T_c value (around 450–500 °C) can be deduced for the granite, north as well as south of the main NW–SE late fault (sample TR420 on Fig. 10).

Hysteresis loops were determined using a translation inductometer within an electromagnet reaching 1.6 T. All the measured loops (Fig. 11a) have a very similar shape, with saturation for field lower than 0.02 T. Some of them are slightly pot-belied, corresponding to samples with several magnetic phases. On a Day plot (Day et al., 1977), most of the data correspond to MultiDomain (MD) grain size for titanomagnetite (Fig. 11b). That is the case for all the samples showing by the $K(T)$ curve a single (or strongly dominant) pure magnetite component. The six samples outside of the MultiDomain (MD) area on this diagram all correspond to samples with several magnetic phases, and have size that cannot be determined using the Day plot for pure titanomagnetite. On this plot, they are however very close to the MD area, showing that at least their pure magnetite component has probably a large size. We can thus expect a magnetic fabric directly related to the shape of the magnetite grains, except for the sites with low susceptibility (Table 4) where this fabric is very probably carried by the paramagnetic minerals.

6.3. Magnetic fabric

The AMS in low field, measured using a KLY3 Kappabridge, yields the principal magnetic susceptibility axes maximum K_1

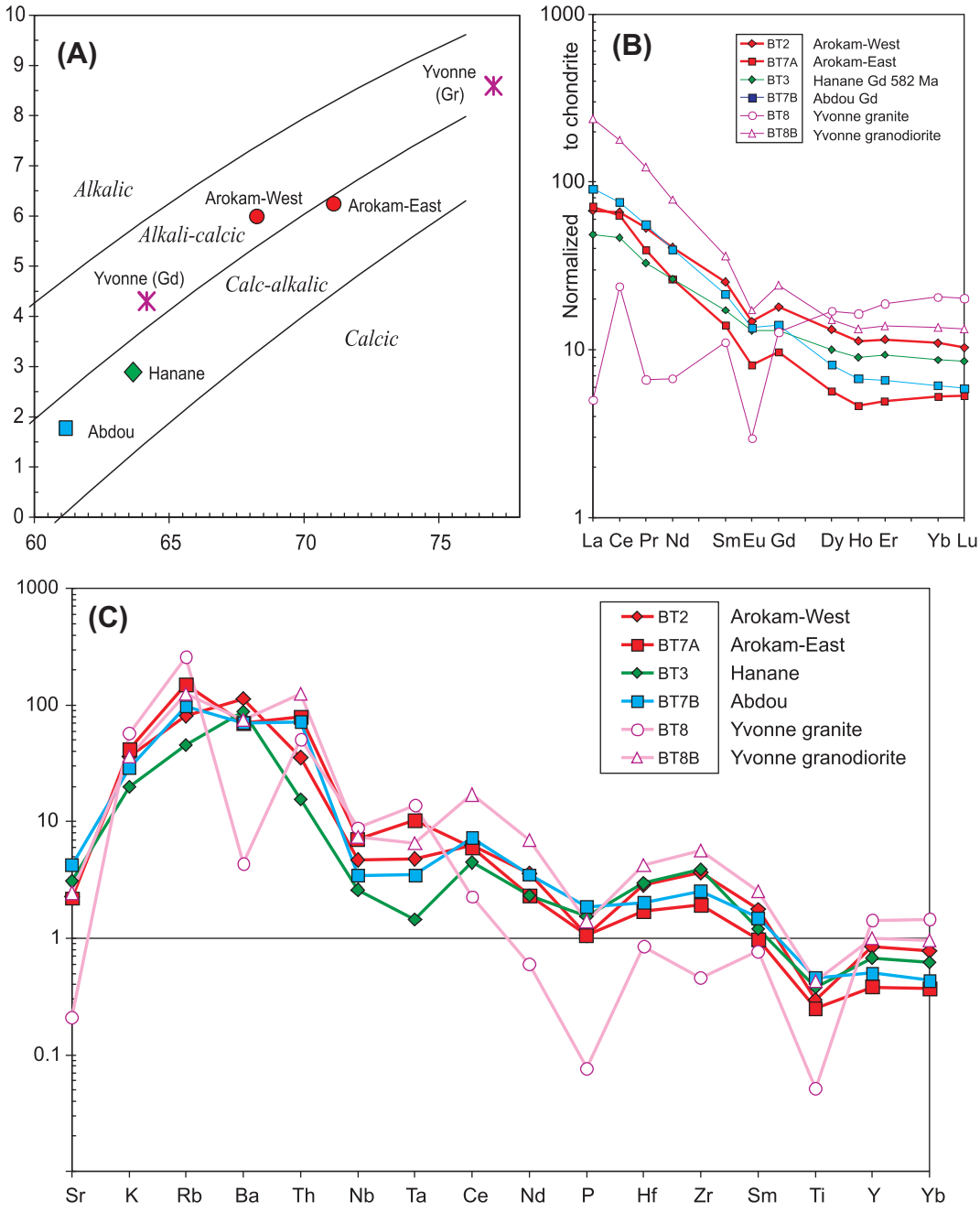

Fig. 7. Geochemical compositions of the studied rocks. (A) MALI (modified alkali-lime index: $Na_2O + K_2O$–aO, wt.%) vs SiO_2 (Frost and Frost, 2008); (B) Rare earth elements normalized to chondrite (Taylor and Mc Lennan, 1985); (C) Incompatible elements normalized to MORB (Sun, 1980; Pearce, 1982).

(magnetic lineation), intermediate K_2 and minimum K_3 (pole of the magnetic foliation). The Jelinek (1981) intensity P' and shape T (possibly varying from +1 for oblate to −1 for prolate) parameters were used to describe the magnetic fabric. The data for a group of samples, at the site scale as well as at the pluton scale, were analyzed using normalized tensor variability (Hext, 1963; Jelinek, 1978), simple bootstrap (Henry, 1997) and bivariate (Henry and Le Goff, 1995) statistics. For bivariate statistics (LeGoff, 1990; Le Goff et al., 1992), weighting by precision parameter k related to measurement uncertainty was applied. The three methods gave here similar results. The magnetic zone axis (Henry, 1997) was determined, with its associated confidence zones at 63% and 95%, in order to obtain indications about the origin (stretching or planes intersection) of the magnetic lineation. Mean tensor data obtained at the pluton scale generally give only a rough indication, being only clearly significant for data from pluton with coherent fabric, as in several of the studied plutons here.

The mean susceptibility in aplitic dykes is mainly weak, except for two sites in the Abdou pluton (sites 67a and 72a where it is relatively higher). In dyke sites 04a and 20a of the Arokam-West pluton, magnetic axes orientations are the same as in host granite. In the site 20a, dyke's P' value is particularly high (1.51 compared to 1.03 in the host granite). This is not the case in all the other dykes in the different studied plutons where P' values are very close to those obtained in granites in the same site. In a same site, the T values are mostly lower in dykes than in granites. The granodioritic dyke (site 16d in the Arokam-West pluton) shows on contrary higher Km (4467×10^{-6} SI) than the granitic host-rock (1645×10^{-6} SI).

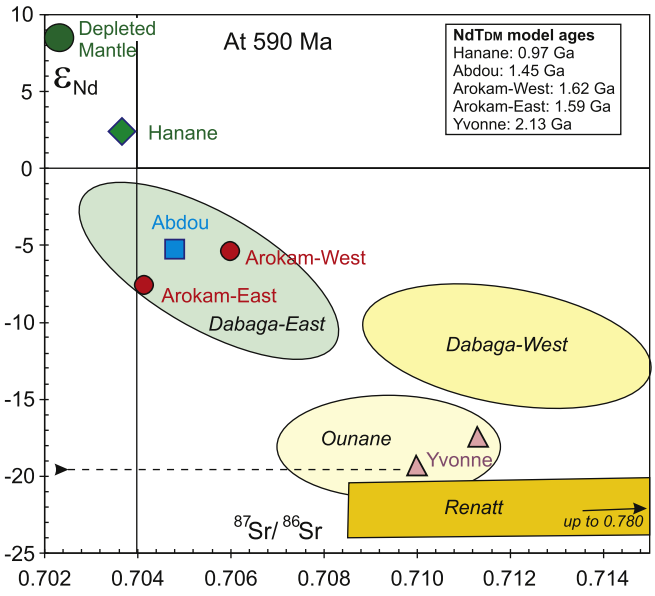

Fig. 8. $^{87}Sr/^{86}Sr$ initial ratios and eNd calculated at 590 Ma for the dated rocks compared to granitoids in the region. Dabaga-East (Liégeois et al., 1994) are granitoids in Aïr to the south, east of the Raghane shear zone. Dabaga-West, and Renatt (Liégeois et al., 1994) are granitoids in Aïr to the south, west of the Raghane shear zone and Ounane (Liégeois et al., 2003) is a granitoids to the north, west of the Raghane shear zone. NdT_{DM} model ages following Nelson and Depaolo (1985). The dotted arrow indicates that the granitic sample has actually a calculated Sr initial ratio < 0.7, due to subsolidus event (see text).

6.3.1. The Arokam-West/Hanane area

The mean susceptibility values (Fig. 10 and 11 and table 4) are in average higher in the Hanane granodiorite (11,140 × 10^{-6} SI) than in the Arokam-West orthogneiss (8455 × 10^{-6} SI). They are very variable according to the site in both cases, the highest values being noted in the Arokam-West sites 5 and 6 (>29,000 × 10^{-6} SI). The average of the susceptibility values appears lower in southern Arokam-West section, but this is mainly related to the sites with high fracturation where the susceptibility has very low values. The site 6 has the highest P' value (1.30) in the northern Arokam-West section, but for the southern Arokam-West section the highest value (1.50) is located in an aplitic dyke (TI 20a) and in the granitic site 21 (P' = 1.22), both in the same high deformation zone. The Hanane sites have P' values between 1.07 and 1.15, not significantly different from that in the Arokam-West sites (between 1.05 and 1.12). The T parameter values are also similar in both types of rocks. They are relatively high in the southern Arokam-West section around 0.60, particularly in the sites showing a visible deformation (sites 18–22). T values in this southern section are all positive while half of sampled sites in the northern Arokam-West section show negative T values.

The magnetic lineation in the Arokam-West orthogneiss has generally a N–S to N040° direction with weak plunge toward the north in the northern section and toward the SSW in the southern one. Some plunge values of lineation are relatively high associated with a N040° orientation. Magnetic foliation in this rock is also N–S with quite high westward plunge in the northern part of the pluton. In the southern part, foliation plunge, mainly toward W to SW, has lower values. In the southern part, the magnetic zone axis

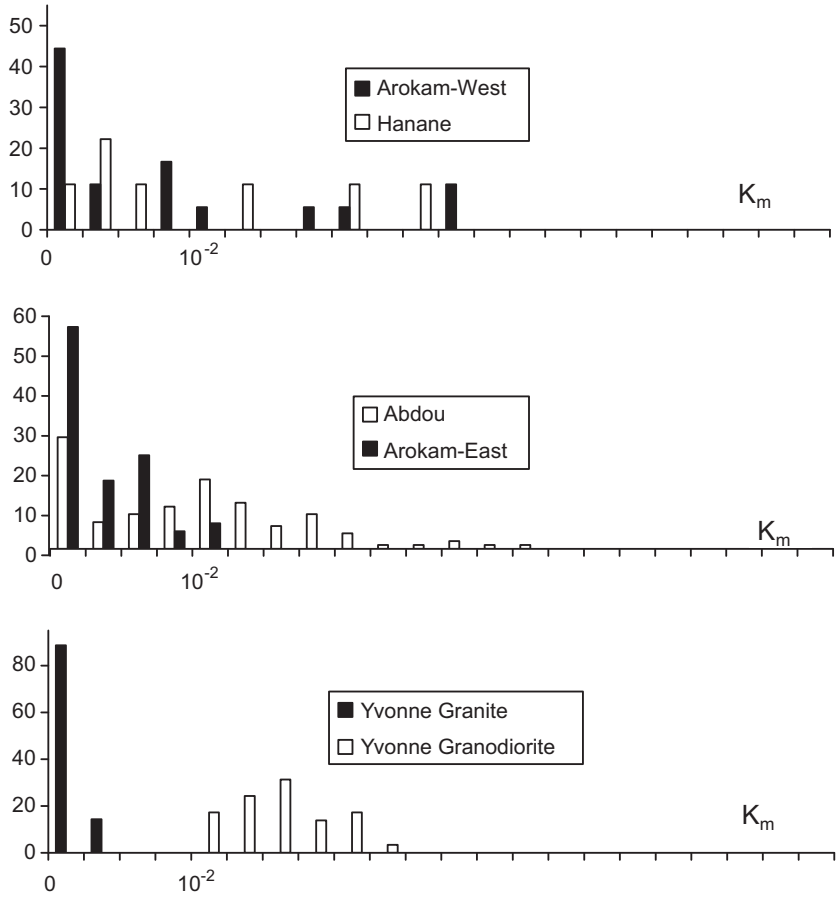

Fig. 9. Column diagrams in percentage (relative frequency) of the mean susceptibility value K_m (in SI) of the samples in the different studied plutons.

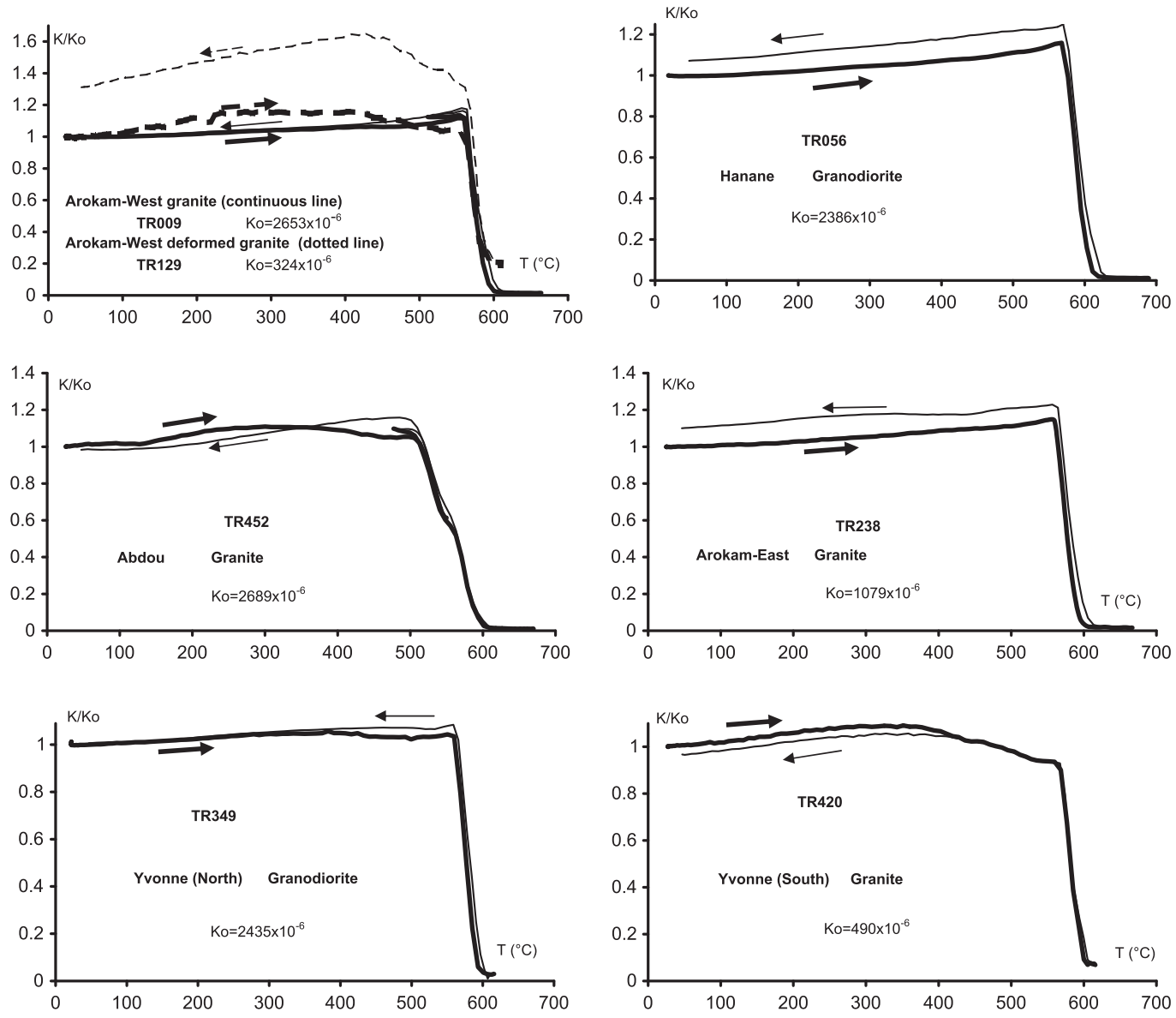

Fig. 10. Examples of normalized thermomagnetic curves of samples from the Arokam-West basement granite (samples TR009 – site Tl02 – and TR129 – site Tl17), Hanane granodiorite (sample TR056 – site Tl09), from Abdou (sample TR452 – site Tl63) and Arokam-East (sample TR238 – site Tl32) plutons, and from Yvonne granite (sample TR420 – site Tl59) and granodiorite (sample TR349 – site Tl48). Curves with indication of the mean susceptibility Ko in SI.

($D = 273°$, $I = 38°$) is significantly different from the mean K_1 axis ($D = 199°$, $I = 34°$).

The magnetic fabric in the Hanane granodiorite presents much more scattered principal directions than in the Arokam-West orthogneiss, though measurement uncertainty is similar in both cases. The mean principal directions (Fig. 12) are however relatively similar in both intrusions.

6.3.2. The Arokam-East/Abdou area

The magnetic fabric in the Arokam-East orthogneiss is similar to that of Arokam-West orthogneiss while the Abdou pluton shows a different magnetic fabric (Figs. 12 and 13 and Table 4).

In the Abdou pluton, the magnetic lineation has in average a high plunge to NE or SW and the pole of magnetic foliation is close to the horizontal plane (Fig. 12). The magnetic fabric is identical in both the Abdou facies (granite and granodiorite). In the Arokam-East orthogneiss, the magnetic lineation shows low values of plunge northward or southward and the magnetic foliation planes have sub-meridian direction with low values of plunge. In both Abdou and Arokam-East units, the magnetic zone axis is not significantly different from the mean K_1 axis. The mean magnetic susceptibility is higher in the Abdou pluton (average of 9080×10^{-6} SI reaching more than $30{,}000 \times 10^{-6}$ in the site 73) than in the Arokam-East orthogneiss where the values have an average of only 3300×10^{-6} SI). The P' values are high in the Abdou pluton, especially in the border sites 73–74 1.20 and in the granodiorites sites 67–72 (mainly over 1.05).

6.3.3. The Yvonne composite pluton

The Yvonne granite (Figs. 12 and 13 and Table 4) shows relatively low values of the mean susceptibility, not exceeding 4190×10^{-6} SI. Some sites (33, 35 and 54–56) toward the NW–SE fault (highly fractured rocks) have even very low values. P' values are relatively low, varying from 1.02 to 1.06. On contrary, in the granodiorite, the mean susceptibility values are quite high ($15{,}460–18{,}238 \times 10^{-6}$ SI) in all the sampled sites (44–48). The P' values are slightly higher between 1.03 and 1.06. The T values are situated in average around 0.50 with positive but also negative

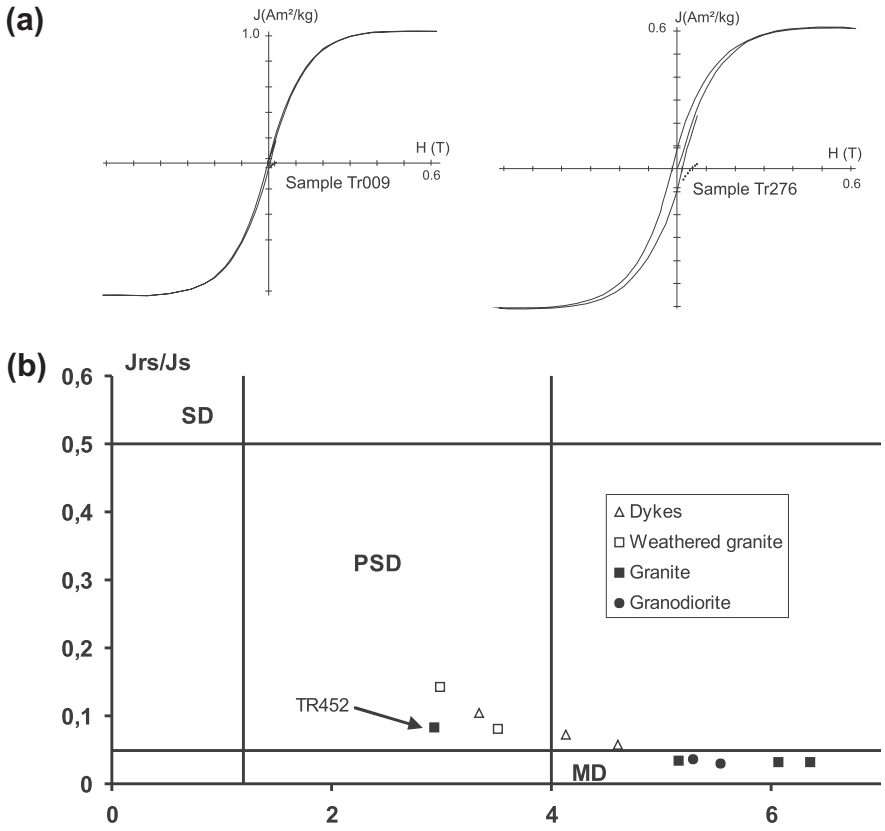

Fig. 11. (a) Hysteresis loop after correction of the paramagnetism showing two typical examples: samples TR009 (granite – site Tl02 in the Arokam-West orthogneiss) and TR276 (dyke – site Tl38a in the Yvonne granite). (b) Day plot (Day et al., 1977) of the hysteresis parameters ratios of different samples showing two (dykes, weathered granite and sample TR452 – site Tl63) or one (other granites and granodiorites) magnetic phases; SD (single domain), PSD (pseudo-single domain) and MD (multidomain).

values. The magnetic lineation in the granite mainly plunges toward north or south with low values; in the southern part of the pluton, it locally shows some weak plunges to SW. The magnetic foliation plane has different directions, mainly with a weak plunge, but with a higher plunge toward NW or SE in the southern part of the pluton (sites 52–58). The granodiorite in the north shows some higher values (around 60°) of the lineation plunges to the WSW and the foliations plunge to NW with high values. In the granite and in the granodiorite, the mean K_1 axis is not significantly different from the magnetic zone axis.

7. Discussion

The Raghane fault is a major dextral strike slip shear zone corresponding to the western boundary of the Saharan metacraton and reactivated several times during the Pan-African period (Black et al., 1994; Liégeois et al., 1994). The regional stress field related to this activity has been recorded by different generations of granites around the shear zone north of the studied area (Henry et al., 2009). How was affected the Arokam Ténéré? Have the studied plutons specific characteristics? What was the structural evolution around the Raghane shear zone in this area? What are the implications for the tectonic history of the Hoggar shield? These points are the main objectives of the following discussion.

7.1. Magnetic fabric-forming conditions

7.1.1. The Eburnean plutons (1.92 Ga) gneissified during the Pan-African (0.58 Ga)

The magnetic fabric of the Arokam-West and -East orthogneiss is independent from the plutons shape appearing on the map (Fig. 2), these shapes being simply a consequence of the effect of the erosion of the overlying Tririne Group, masking most of the Arokam orthogneiss. This fabric is similar to that already obtained in most Pan-African plutons around the Raghane shear zone, especially a well-developed N–S to NNE–SSW magnetic lineation with weak plunge (Henry et al., 2009). In the Arokam-West sites 5 and 6, a preferential orientation of the enclaves lengthening has been observed and indicates the magma flow direction. K_1 and K_1 axes have a direction different from this preferential orientation. The magnetic fabric therefore does not reflect the Eburnean magma flow, but is related to the regional stress field in relation with the Pan-African movements along the Raghane shear zone. In the southern part of the Arokam-West orthogneiss, deformations related to late brittle movements along NNE–SSW faults occurred, corresponding to conjugate movements associated with the Raghane shear zone. The magnetic fabric coincides with the visible deformational fabric. The flattening is clearly dominant in the most deformed orthogneiss. Moreover, the difference between mean K_1 axis and magnetic zone axis indicates that K_1 is here related to a mineral lineation (Henry, 1997). The magnetic fabric reflects then the deformation during an episode of the activity of the Pan-African Raghane shear zone when the Arokam complex was cold.

7.1.2. The Pan-African Hanane pluton (0.58 Ga)

The magnetic fabric of the Hanane granodiorite is similar to that of most plutons studied and has the same origin, i.e. related to the regional stress field in relation with the movements along the Raghane shear zone. Except very close to the pluton border, no shape preferential orientation of the main minerals has been observed. No evidence of post-magmatic deformations has been found in all the studied sites. The magnetic anisotropy is however relatively strong (mean P' value of 1.10). The magnetic fabric is therefore related to the structural conditions that occurred during

Table 4
Site, Number of core-samples (N), mean susceptibility in 10–6 SI (km), declination (D_1) and inclination (I_1) of the magnetic lineation – i.e. K_1 axis, declination (D_3) and inclination (I_3) of the normal to the magnetic foliation – i.e. K_3 axis, parameters P' and T (Jelinek, 1981). Normal, bold and italic characters indicate sites in granite, granodiorite and aplitic dykes respectively. (∗) corresponds to sites showing clear post-magmatic deformation. Indications "a" and "d" in the site name correspond to aplite and diorite respectively.

Site	N	K_m	$D_1°$	$I_1°$	$D_3°$	$I_3°$	P'	T
Arokam-West orthogneiss								
TI01	8	8349	347	33.1	109.9	40	1.064	−0.61
TI02	6	18,683	21.2	42.4	120.4	9.9	1.135	−0.28
TI03	8	9107	347	13	81.4	20.6	1.09	0.31
TI04	2	1693	345.5	48.6	94.6	16.1	1.046	0.71
TI04a	*5*	*600*	*350.8*	*13.4*	*93.8*	*43.2*	*1.024*	*−0.12*
TI05	6	29,868	20.3	45.6	121.5	10.7	1.145	−0.14
TI06	6	29,488	0.3	8.8	92.3	12.6	1.302	0.09
TI11	6	1785	345	35.9	125.4	46.8	1.057	0.37
TI12	10	1424	298	44.5	181	25.2	1.06	−0.28
TI13	7	22,366	4.3	8.5	96.5	14.1	1.229	0.53
TI15d	9	6641	205	10.3	93.6	62.8	1.085	0.16
TI16	7	1645	11	4.9	105.7	43.5	1.063	0.55
TI16d	7	4467	353.5	6.3	101.7	70.6	1.072	0.15
TI17	7	3962	11.7	0.6	102.7	61.5	1.171	0.09
TI18∗	6	219	231	64.8	28.3	23.6	1.09	0.51
TI19∗	6	153	199	31.1	73.2	43.5	1.072	0.65
TI20∗	6	141	193	45	42.8	40.8	1.039	0.64
TI20a∗	*6*	*20*	*297*	*45.7*	*47.9*	*19.5*	*1.512*	*0.58*
TI21	6	2321	203	41.9	15.8	47.9	1.221	0.44
TI22	6	1600	161.9	22.7	39.3	52.3	1.078	0.73
TI23	6	9197	186	59.7	42.6	25	1.168	0.2
TI24	7	10,189	213	46.4	85.9	29.5	1.195	0.41
Arokam-East orthogneiss								
TI25	7	2035	37.7	72	266	12.2	1.015	0.57
TI25a	*6*	*702*	*68.3*	*65.9*	*269.3*	*22.7*	*1.013*	*−0.33*
TI26	6	1416	10.9	19.4	107.3	17.4	1.03	0.31
TI27	6	1253	192	4.1	282	6.5	1.018	0.27
TI27a	*6*	*866*	*32.8*	*1.2*	*123*	*9.7*	*1.096*	*0.16*
TI28	8	2030	204	11.9	295	4.4	1.045	−0.78
TI29	6	5492	199	6	105.7	27.7	1.045	0.33
TI30	6	5514	191	1.1	98.8	49.2	1.054	0.11
TI31	6	4985	191	4	96.4	43.4	1.046	0.4
TI32	7	9324	346	9.9	94.8	62.5	1.051	0.03
Hanane pluton								
TI07	6	1632	335	4.9	65.6	11.3	1.11	−0.18
TI08	8	2823	14.3	62.5	275	5.2	1.158	0.06
TI09	8	21,629	356	9.4	261	29.4	1.158	−0.32
TI10	7	26,921	343	8.3	107.8	5.6	1.076	0.33
TI14	8	13,480	201	22.3	105.7	11.5	1.102	0.75
Abdou pluton								
TI60	6	11,016	83.2	81.9	324	4	1.174	−0.23
TI60a	*6*	*1496*	*35.2*	*22.4*	*297.2*	*18.6*	*1.099*	*0.6*
TI61	6	2846	239	85.9	125	1.6	1.05	0.04
TI62	7	1450	68.5	30.8	299	47.1	1.038	0.57
TI63	6	12,708	85.8	62.2	294	25	1.064	−0.41
TI64	6	920	228	68.4	116.9	7.9	1.028	0.45
TI65	6	750	35.6	63.7	267	17.4	1.019	−0.25
TI66	6	13,190	40.3	39.4	305	7.5	1.146	0.62
TI67	6	9644	49.4	32.2	310	14.7	1.055	0.56
TI67a	*6*	*4000*	*32.5*	*50.9*	*263.5*	*27*	*1.04*	*−0.32*
TI68	6	9731	54.6	43.2	323.2	1.5	1.05	0.14
TI69	6	6272	252	62.4	7.7	13	1.05	0.2
TI70	6	17,910	141.3	44.6	48.4	2.9	1.188	0.41
TI71	6	10,926	123	61.6	21	6.4	1.139	0.37
TI72	6	12,270	328.5	60.7	207.1	11.5	1.115	0.83
TI72a	*6*	*8250*	*289*	*80*	*39.7*	*3.6*	*1.129*	*0.6*
TI73	8	30,233	335	65.5	225	8.9	1.24	0.62
TI74	7	18,580	351.1	35.2	82.8	2.4	1.236	0.39
TI75	6	11,498	206	80	323	4.5	1.087	0.87
TI76	6	1776	89	9.2	358.7	2.2	1.12	0.62
TI77	7	5292	89	53.3	306	30.9	1.043	−0.18
Yvonne granite								
TI33∗	6	35	17	13.6	152.3	71.2	1.027	0.77
TI34	6	1140	187	14	319	69.5	1.052	0.27
TI35	*6*	*60*	*221*	*26.4*	*351*	*52.3*	*1.066*	*0.37*
TI36	6	1310	191	2.9	99.6	10.1	1.04	−0.26
TI37	7	190	197	14.9	287	0.8	1.05	0.19
TI38	6	1631	358.9	61.4	203	26.5	1.044	−0.16
TI38a	*6*	*406*	*40.6*	*31.9*	*172.6*	*47.1*	*1.013*	*0.66*
TI39	6	1631	197	4.4	104.2	25.2	1.026	−0.06
TI40	7	710	4.2	7	232	79.8	1.027	0.19
TI41	6	528	347	16.3	88.7	35.1	1.018	0.12
TI42	6	140	23.4	11	215	78.8	1.048	0.02
TI43	*6*	*14*	*128*	*18.1*	*228*	*27.5*	*1.025*	*−0.68*
TI49	6	2128	223	0.4	132.1	17.3	1.045	−0.1
TI50∗	6	343	188	26.3	313	49	1.064	−0.22
TI51	6	2144	19.4	51.3	114.1	3.7	1.037	−0.06
TI52	7	2617	37.8	13.1	129.3	6.4	1.059	−0.5
TI53	6	2021	37.1	18	128.2	3.4	1.056	−0.9
TI54∗	6	33	60.1	37.3	170	24.1	1.035	−0.42
TI55∗	6	48	31.5	13.2	191	76	1.024	0.25
TI56∗	6	47	17.8	3.9	149.6	84.1	1.036	0.5
TI57	6	2366	29.9	0.9	299	58.1	1.089	−0.51
TI58∗	6	284	28.5	10.1	120.7	11.9	1.038	0.1
TI59	7	4190	221	5.3	127.2	32.1	1.059	−0.63
TI59a	*6*	*21*	*140.6*	*1.8*	*172.6*	*47.1*	*1.079*	*0.38*
Yvonne granodiorite								
TI44	6	16,017	218	1.4	122.8	73.1	1.035	−0.09
TI45	6	16,005	258	0.2	167.1	13.9	1.062	0.46
TI46	6	15,460	258.2	42.2	135.8	30.4	1.066	0.26
TI47	7	15,269	314	57.6	127.8	32.3	1.066	0.04
TI48	6	18,238	164	36.6	93.7	53	1.052	0.41

the late-magmatic evolution of the pluton. The relative scattering of the principal axes suggests moderate effect of these conditions, probably because the Arokam-West orthogneiss, in which the granodiorite intruded, acted as a rigid block, partly protecting the granodiorite from the regional deformation (Henry et al., 2008).

7.1.3. The Pan-African Abdou pluton

In site 66, a preferential orientation of the enclaves lengthening has been observed. K_1 axes are parallel to this orientation and then still reflect the magma flow. K_1 axes in the different sites have mostly relatively high plunge. Such an orientation of K_1 axes, subvertical and linked to magma flow is very different from that of almost all the other studied plutons in the Hoggar where the fabric is related to regional stress field. Only a part of the Tihaliouine pluton in Central Hoggar (late Taourirt pluton; Azzouni-Sekkal et al., 2003) has a similar structure (Henry et al., 2008). The orientation of the magnetic foliation, often with steep plunge, is rather related to that of the pluton border. All the characteristics indicate that the magnetic fabric here still corresponds to the magma emplacement and was not tectonically disturbed during the late-magmatic period. The Abdou pluton intruded the same country-rocks as the Hanane pluton and it cannot be claimed for a difference of the regional rheology as in the case of the Teg Orak pluton (Henry et al., 2008). The most likely explanation is that Abdou intruded later than Hanane, when the regional stress field was vanishing.

7.1.4. The Pan-African Yvonne composite pluton (0.595 Ga)

The magnetic fabric of *the Yvonne granite* is similar to that of most plutons studied and has the same origin. The granite is cut by a major NW–SE fault but its magnetic fabric close to the fault is not different from that in the other sites and was therefore not disturbed during the fault activity that is clearly post-magmatic. This is different from the case of the NNE–SSW faults observed in the Arokam-West massif and where the magnetic fabric is related to post-magmatic movements along the faults. This NW–SE fault is probably related to the younger Murzukian event that occurred to the east (570–550 Ma; Fezaa et al., 2010), generating here only

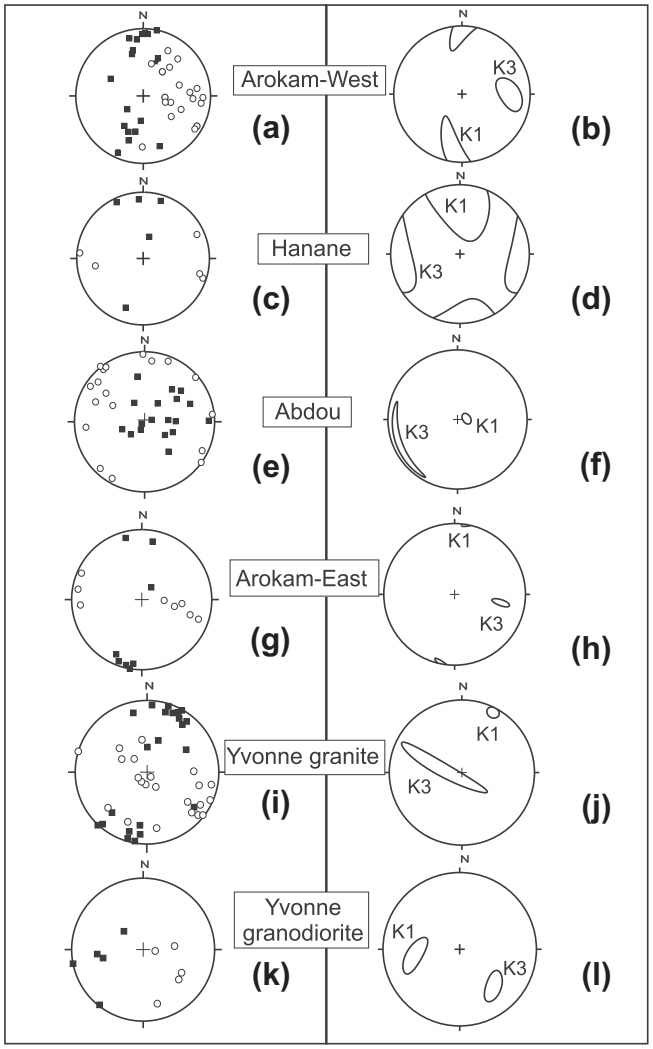

Fig. 12. Maximum (K_1, squares) and minimum (K_3, circles) principal magnetic susceptibility axes of the samples from the Arokam-West basement granite (a), Hanane granodiorite (c), the Abdou (e) and Arokam-East (g) plutons, and the Yvonne granite (I) and granodiorite (k) (stereographic projection in the lower hemisphere). Confidence zone at 95% (Hext, 1963; Jelinek, 1978 for the principal susceptibility axes maximum K_1 (squares) and minimum K_3 (circles) of the samples from the Arokam-West basement granite (b), Hanane granodiorite (d), the Abdou (f) and Arokam-East (h) plutons and the Yvonne granite (j) and granodiorite (stereographic projection in the lower hemisphere).

brittle faults even possibly accompanied by fluids as suggested by Sr isotopes (see above).

The Yvonne granodiorite shows a different fabric, very similar to that of the previously studied syntectonic 0.59 Ga Ohergehem pluton (Henry et al., 2009). The latter represents a magmatism contemporaneous to the main movements along the Raghane shear zone. That was the period of the main northward movement of the Assodé-Issalane terrane along the western boundary of the Saharan metacraton, only affected by secondary thrust structures along the Raghane shear zone (Liégeois et al., 1994). The similarity of the magnetic fabric in the Ohergehem (dated at 594 ± 4 Ma – Henry et al., 2009) and Yvonne granodiorites suggests a similar age. This implies an age difference between emplacement of the Yvonne granodiorite and of granite that are structurally independent intrusions. The age obtained for the Yvonne granite (595 ± 3 Ma) is however the same as that of the Ohergehem pluton, indicating a rapid switch in stress field, suggesting that the age of 595 Ma probably dates the end of the main northward movement of the Assodé-Issalane terrane.

7.2. Structural implications

The basement of the Saharan metacraton in Eastern Hoggar was not known before this study. Only the Djanet Group, equivalent to the Tririne Group bears Archean and Paleoproterozoic detrital zircons (Fezaa et al., 2010) and one inherited zircon with an age of 1.83 Ga has been measured in the *c.* 800 Ma old Oued Touffok pluton (Henry et al., 2009), but all these zircons have been interpreted as coming from Central Hoggar, largely made of Paleoproterozoic lithologies (Bendaoud et al., 2008). Only the rare Paleoproterozoic inherited zircon cores present in the Djanet intrusions suggested the presence of an old basement at depth (Fezaa et al., 2010). An old rigid basement to the east of the Raghane shear zone was inferred by Liégeois et al. (1994) for explaining the contrasted behavior on both sides of the shear zone. Arokam-West and -East orthogneiss represent the first known occurrences of this rigid basement, which is Eburnean in age. In this Arokam orthogneiss, the magnetic fabric is related to solid-state deformation on a cold body. The similarity of this fabric with that affecting the Pan-African Hanane granodiorite indicates its Pan-African age. The relative low intensity of this deformation and its strong lateral variability agree with the transpressive regime of the Raghane shear zone and confirms that the Arokam basement acted as a rigid block during the Pan-African times. The presence of this rigid basement explains why the overlying Tririne Group is only weakly deformed, despite the intensity of the deformation along the Raghane shear zone, confirming the hypothesis made for eastern Aïr and the same Aouzegueur terrane by Liégeois et al. (1994).

The similarity of the magnetic structures of the Yvonne and Oherghem granodiorites suggests that the same structural conditions existed around 600 Ma on both sides of the Raghane shear zone, in the Assodé-Issalane terrane and in the Aouzegueur terrane (Saharan metacraton) during the main activity of the Raghane shear zone, implying the development of secondary thrusts on both sides of this shear zone. Thrusts have been indeed described west of the Raghane shear zone in Aïr, especially in the Agalen area (Liégeois et al., 1994). The contrasted Sr and Nd isotopic signature of the Yvonne pluton on the one hand and the Hanane and Abdou plutons on the other hand, confirms that the Raghane shear zone separates two distinctive lithospheres.

In the Hoggar shield, almost all the Pan-African plutons studied by AMS present a strong magnetic fabric with subhorizontal magnetic lineation having an orientation related to that of the neighboring shear zones (Henry et al., 2009 and reference therein), implying the absence of significant post-magmatic deformation. This is the case for the Hanane granodiorite and Yvonne granite, implying that their magnetic fabric relates to the regional stress field during the late-magmatic period, when most magnetite crystallized. This points out that the main activity of the Raghane shear zone was almost continuous, because local distensions due to this activity allowing the magma intrusion never remained for a long time. This is in agreement with the model where the Raghane shear zone resulted from the northward motion of the Assodé-Issalane terrane along the western boundary of the Saharan metacraton (Liégeois et al., 1994).

Concerning the magnetic fabric, the Abdou pluton is an exception: it is one of the two known plutons in Hoggar (with Tihalioune pluton in Central Hoggar – Henry et al., 2008) that was not submitted to a regional stress field during its late-magmatic phase. This is probably due to the combination of the rigidity of the Arokam basement and to a young age of this intrusion. Still undated, we can predict an age younger than 580 Ma for Abdou pluton.

The late tectonic evolution in the area can be depicted. The late evolution of the different fault networks in the Arokam Ténéré comprises two successive events marked by important faults distinct from the Raghane main structure. A common feature is that

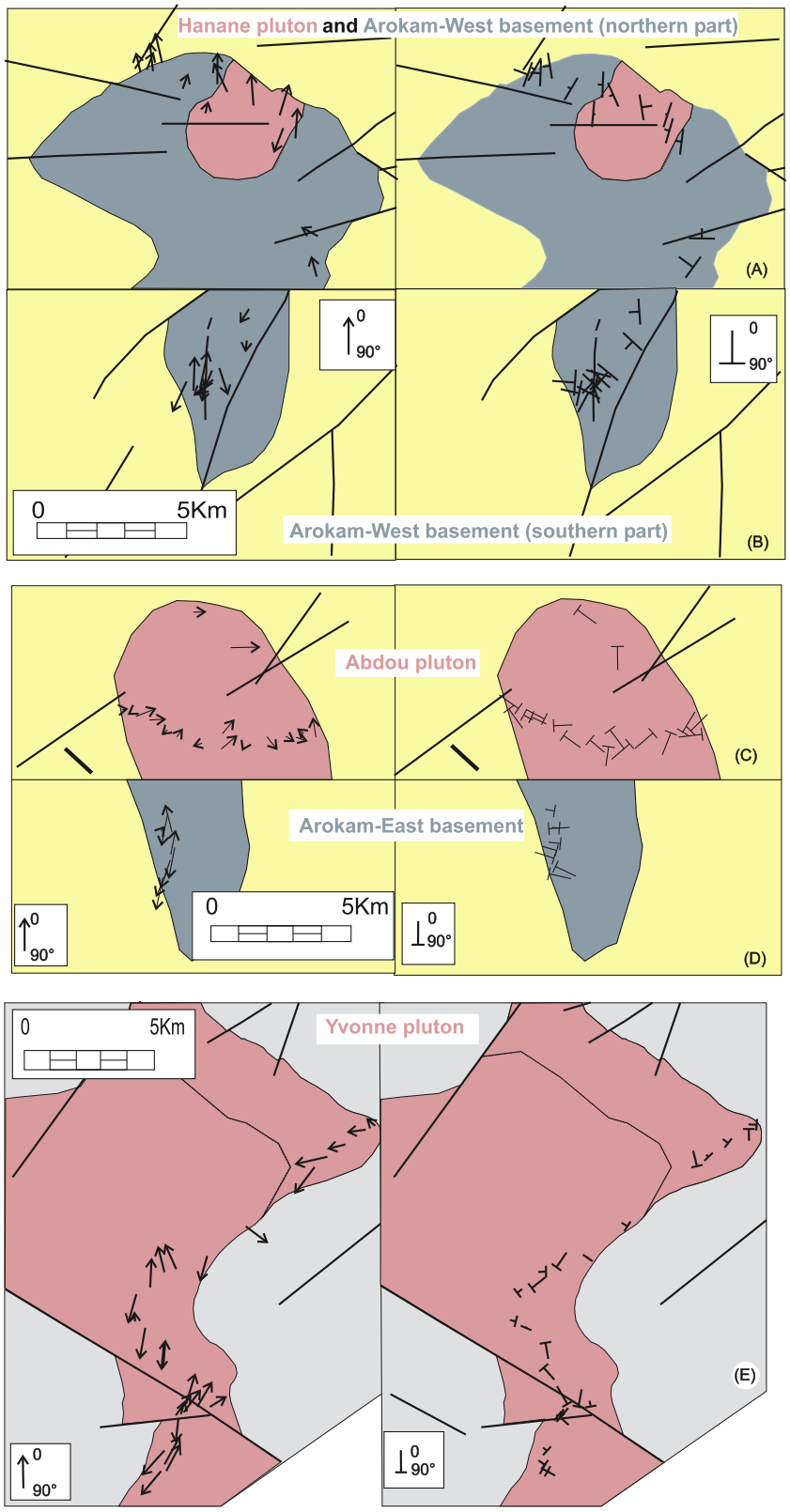

Fig. 13. Maps of northern (A) and southern (B) parts of the Hanane – Arokam-West massif, Abdou (C), Arokam-East (D) and Yvonne (E) plutons with the distribution of the magnetic lineation (left side) and magnetic foliation (right side) measured in the studied sites. The length of the symbols (arrow for lineation, plunge indication for foliation) is proportional to the plunge values (scale on the figure).

in the vicinity of the two generations of faults, the rocks are highly fractured, favoring a strong weathering marked in particular by a strong mean susceptibility decrease. In the Hanane pluton, the rock is slightly deformed along NNE–SSW faults and the magnetic fabric is related to the deformation. In the Yvonne granite, the well-visible NW–SE fault does not induce any magnetic fabric. This suggests that two faults have had a different evolution and likely do not belong to a same conjugated network. The NNE–SSW faults

reflect most probably, like in the Tiririne area (Henry et al., 2009), an effect of the blocking of the N–S Raghane shear zone with fault activity transferred to another fault network. The NW–SE fault, that shifted the Raghane shear zone in northern Niger, is mainly a very late Pan-African structure, maybe linked to the Murzukian event that occurred to the east between 575 and 555 Ma (Fezaa et al., 2010).

8. Conclusion

In the Arokam Ténéré (Aouzegueur terrane, south-eastern Hoggar), east of the Raghane mega-shear zone, we have found for the first time in Eastern Hoggar the Eburnean basement of the Saharan metacraton: the Arokam orthogneiss has been dated at 1918 ± 5 Ma by the U–Pb LA-ICP-MS method on zircon. It has been moderately gneissified during the Pan-African orogeny, some of its zircons having recrystallized thin rims tentatively dated at 580 ± 26 Ma, i.e. at the time when plutons intruded, such as the studied elliptical Hanane pluton (582 ± 3 Ma). This Pan-African reworking was moderate, the Arokam protolith (Eburnean granitic pluton) being well preserved in several places. On the other side of the Raghane shear zone, in the Assodé-Issalane terrane, the Yvonne elliptical pluton has been dated at 595 ± 3 Ma.

Geochemically and isotopically (Sr and Nd isotopes), the Eburnean Arokam orthogneiss and the Hanane and Abdou plutons share many similarities suggesting a similar lithospheric source, the Eburnean source being remelted during the Pan-African orogenies. This signature is comparable to the Dabaga-East granitoids to the south in Aïr that also intruded to the east of the Raghane shear zone (Liégeois et al., 1994). This agrees with a metacratonic setting (Liégeois et al., 2003; De Waele et al., 2006; Ennih and Liégeois, 2008). By contrast, the Yvonne geochemical and isotopic signature is strongly distinct (alkali-calcic and much more negative ε_{Nd}), being similar to the various Pan-African intrusion of the Assodé-Issalane terrane, west of the Raghane shear zone (Liégeois et al., 1994).

The comparison of magnetic fabric of the studied intrusions with that previously obtained along the Raghane shear zone (Henry et al., 2009) emphasizes the occurrence of different groups of plutons. The Eburnean Arokam gneissic pluton has deformational magnetic fabric likely related to the Pan-African orogeny. The Yvonne and Ohergehem granodiorites, though located in two different domains of the Hoggar shield (Assodé-Issalane terrane and Aouzegueur terrane belonging to the Saharan metacraton, respectively), but both dated at *c.* 595 Ma, display structures linked to secondary thrusts, as it is the case of the Dabaga-East plutons in Aïr (Liégeois et al., 1994), which have been considered as syn-thrust (Liégeois et al., 1998). These thrusts were associated with the large movements that occurred along the Raghane shear zone.

The younger Hanane pluton (582 ± 3 Ma) intruded during a less important activity of the Raghane shear zone but its magnetic fabric is still entirely due to the regional stress field, late magmatic structures having totally overprinted the emplacement fabric, similarly to the Yvonne granite. Considering that the emplacement of the plutons was favored by local distensions (e.g. Guineberteau et al., 1987; Tikoff and Teyssier, 1992) related to movement along shear zones, this implies a protracted activity of the Raghane shear zone.

The Abdou pluton remarkably departs from the Yvonne and Hanane plutons, as from all except one plutons in Hoggar: its magnetic fabric still shows the initial fabric related to magma emplacement, with subvertical magnetic lineation, indicating that this pluton kept recorded the distension conditions that occurred during its late-magmatic evolution.

The late faults, well visible as they induced a strong weathering of the rocks, are marked by a strong mean susceptibility decrease. This study indicates the existence of two successive generations of faults. The first one is oriented NNE–SSW and induced a localized magnetic fabric in the Hanane pluton. The second one, NW–SE oriented, although being spectacular did not induce any magnetic fabric. The latter one, that shifted the Raghane shear zone in Niger, is a very late Pan-African structure, maybe linked to the Murzukian event that occurred to the east between 575 and 555 Ma (Fezaa et al., 2010).

Acknowledgements

This project is supported by the PICS cooperation program "Architecture lithosphérique et dynamique du manteau sous le Hoggar". We thank G. Borradaile and an anonymous reviewer for their positive advice on this paper, which has been greatly appreciated. We are very grateful to Hicham Bendjeloul, to the civil and military authorities to the "Office de la Recherche Géologique et Minière" (ORGM) and to the "Office du Parc National de l'Ahaggar" (OPNA), all based at Tamanrasset, for their help.

References

Abdelsalam, G., Liégeois, J.P., Stern, R.J., 2002. The Saharan Metacraton. Journal of African Earth Sciences 34, 119–136.

Acef, K., Liégeois, J.P., Ouabadi, A., Latouche, L., 2003. The Anfeg post-collisional Pan-African high-*K* calc-alkaline batholith (Central Hoggar, Algeria), result of the LATEA microcontinent metacratonization. Journal of African Earth Sciences 37, 295–311.

Archanjo, C.J., Bouchez, J.L., Corsini, M., Vauchez, A., 1994. The granite pluton of Pombal: magnetic fabric and place within the Brasiliano strike-slip tectonics of NE-Brazil. Journal of Structural Geology 16, 323–335.

Arène, J., Blaise, J., Bourgeois, M., Bouvet, M., Byramjee, R., Guérangé, B., Illy, P., Reboul, C., Roche, J., Vialon, P., Lelubre, M., 1961. Geological map "Tazrouk". Bureau de Recherches Minières de l'Algérie and Bureau de Recherches Géologiques et Minières.

Auréjac, J.B., Gleizes, G., Diot, H., Bouchez, J.L., 2004. Le complexe granitique de Quérigut (Pyrénées, France) réexaminé par la technique de l'ASM: un pluton syntectonique de la transpression dextre hercynienne. Bulletin de la société géologique de France 175, 157–174.

Azzouni-Sekkal, A., Liégeois, J.-P., Bechiri-Benmerzoug, F., Belaidi-Zinet, S., Bonin, B., 2003. The "Taourirt" magmatic province, a marker of the closing stage of the Pan-African orogeny in the Tuareg Shield: review of available data and Sr–Nd isotope evidence. Journal of African Earth Sciences 37, 331–350.

Bau, M., 1996. Controls on the fractionation of isovalent trace elements in magmatic and aqueous systems. Evidence from Y/Ho, Zr/Hf and lanthanide tetrad effect. Contribution to Mineralogy and Petrology 123, 323–333.

Bendaoud, A., Ouzegane, K., Godard, G., Ligeois, J.P., Kienast, J.R., Bruguier, O., Drareni, A., 2008. Geochronology, metamorphic P–T–X evolution of the Eburnean granulite-facies metapelites of Tidjenouine (Central Hoggar, Algeria): witness of the LATEA metacratonic evolution. In: Ennih, N., Liegeois, J.P. (Eds.), The Boundaries of the West African Craton. Geological Society, London, Special Publications 297, pp. 111–146.

Bertrand, J.M.L., Caby, R., Ducrot, J., Lancelot, J., Moussine-Pouchkine, A., Saadallah, A., 1978. The late Pan-African intracontinental fold belt of the eastern Hoggar (central Sahara, Algeria): geology, structural development, U/Pb geochronology, tectonic implications for the Hoggar shield. Precambrian Research 7, 349–376.

Bertrand, J.M.L., Michard, A., Boullier, A.M., Dautel, D., 1986. Structure and U/Pb geochronology of Central Hoggar (Algeria): a reappraisal of its Pan-African evolution. Tectonics 5, 955–972.

Black, R, Jaujou, M., Pellaton, C. 1967. Notice explicative sur la carte géologique de l'Aïr à l'échelle 1/500 000e. République du Niger, Direction des Mines et de la Géologie and Bureau de la Recherche Géologique et Minière, Paris.

Black, R., Latouche, L., Liégeois, J.-P., Caby, R., Bertrand, J.M., 1994. Pan-African displaced terranes in the Tuareg shield (Central Sahara). Geology 22, 641–644.

Blaise, J., 1961. Sur la stratigraphie des séries anté-cambriennes dans la région du Tafassasset moyen (Ahaggar oriental). Bulletin de la Société Géologique de France III, 184.

Borradaile, G.J., Kehlenbeck, M.M., 1996. Possible cryptic tectono-magnetic fabrics in "post-tectonic" granitoid plutons of the Canadian shield. Earth Planetary Science Letters 137, 119–127.

Bouchez, J.L., 2000. Anisotropie de susceptibilité et fabrique des granites. Comptes Rendus de l'Académie des Sciences, Paris, Earth Planetary Sciences 330, 1–14.

Bruguier, O., Telouk, P., Cocherie, A., Fouillac, A.M., Albarede, F., 2001. Evaluation of Pb–Pb and U–Pb laser ablation ICP-MS zircon dating using matrix-matched calibration samples with a frequency quadrupled (266 nm) Nd-YAG laser. Geostand. Newsl. 25, 361–373.

Caby, R., Andreopoulos-Renaud, U., 1987. Le Hoggar oriental, bloc cratonisé à 730 Ma dans la chaîne pan-africaine du nord du continent africain. Precambrian Research 36, 335–344.
Day, R., Fuller, M., Schmidt, V.A., 1977. Hysteresis properties of titanomagnetites: grain size and compositional dependence. Physics of the Earth and Planetary Interior 13, 260–267.
De Waele, B., Liégeois, J.P., Nemchin, A.A., Tembo, F., 2006. Isotopic and geochemical evidence of Proterozoic episodic crustal reworking within the Irumide belt of South-Central Africa, the southern metacratonic boundary of an Archaean Bangweulu craton. Precambrian Research 148, 225–256.
Djouadi, M.T., Bouchez, J.L., 1992. Structure étrange du granite du Tesnou (Hoggar, Algérie). Comptes Rendus de l'Académie des Sciences, Paris 315 (II), 1231–1238.
Djouadi, M.T., Gleizes, G., Ferré, E., Bouchez, J.L., Caby, R., Lesquer, A., 1997. Oblique magmatic structures of two epizonal granite plutons, Hoggar, Algeria: late orogenic emplacement in a transcurrent orogen. Tectonophysics 279, 351–374.
Ennih, N., Liégeois, J.P., 2008. The boundaries of the West African craton, with a special reference to the basement of the Moroccan metacratonic Anti-Atlas belt. In: Ennih, N., Liégeois, J.P. (Eds.), The Boundaries of the West African Craton. Geological Society, London, Special Publications 297. p. 117.
Fezaa, N., Liégeois, J.-P., Abdallah, N., Cherfouh, E.H., De Waele, B., Bruguier, O., Ouabadi, A., 2010. The Djanet terrane (Eastern Hoggar, Algeria), the Pan-African metacratonic boundary of the Murzuq craton: field, detrital and magmatic U–Pb zircon and Sr–Nd isotopes evidences. Precambrian Research 180, 299–327.
Fomine, A., 1990. Field map of Tadoumet, Office national de la Recherche Géologique et Minière (ORGM), unpublished.
Frost, B.R., Frost, C.D., 2008. A geochemical classification for feldspathic igneous rocks. Journal of Petrology 49, 1955–1969.
Georgiev, N., Henry, B., Jordanova, N., Froitzheim, N., Jordanova, D., Ivanov, Z., Dimov, D., 2009. The emplacement mode of Upper Cretaceous plutons from the Southwestern part of the Sredna Gora Zone (Bulgaria): structural and AMS study. Geologica Carpathica 60, 15–33. doi:10.2478/v10096-009-0001-8.
Goldstein, S.L., O'Nions, R.K., Keith, R., Hamilton, P.J., 1984. A Sm–Nd isotopic study of atmospheric dusts and particulates from major river systems. Earth Planetary Science Letters 70, 221–236.
Guérangé, B., Vialon, P., 1960. Le Pharusien du bassin de Djanet dans la région du Tafassasset moyen (Ahaggar oriental, Sahara central). Comptes Rendus Sommaire des Séances de la Société Géologique de France 3, 557–559.
Guineberteau, B., Bouchez, J.L., Vigneresse, J.L., 1987. The Mortagne pluton (France) emplaced by pull apart along a shear zone: structural and gravimetric arguments, regional implications. Geological Society of America Bulletin 99, 763–770.
Henry, B., 1974. Sur l'anisotropie de susceptibilité magnétique du granite récent de Novate (Italie du Nord). Comptes Rendus de l'Académie des Sciences, Paris 278C, 1171–1174.
Henry, B., 1997. The magnetic zone axis: a new element of magnetic fabric for the interpretation of the magnetic lineation. Tectonophysics 271, 325–329.
Henry, B., Le Goff, M., 1995. Application de l'extension bivariate de la statistique de Fisher aux données d'anisotropie de susceptibilité magnétique: intégration des incertitudes de mesure sur l'orientation des directions principales. Comptes Rendus de l'Académie des Sciences, Paris 320 (II), 1037–1042.
Henry, B., Djellit, H., Bayou, B., Derder, M.E.M., Ouabadi, A., Merahi, M.K., Baziz, K., Khaldi, A., Hemmi, A., 2004. Emplacement and fabric-forming conditions of the Alous-En-Tides granite, eastern border of the Tin Serririne/Tin Mersoï basin (Algeria): magnetic and visible fabrics analysis. Journal of Structural Geology 26, 1647–1657.
Henry, B., Derder, M.E.M., Bayou, B., Ouabadi, A., Belhai, D., Hemmi, A., 2006. Magnetic fabric of Late Panafrican plutons in the Tamanrasset area (Hoggar shield, Algeria) and structural implications. Africa Geosciences Review 13, 41–52.
Henry, B., Bayou, B., Derder, M.E.M., Djellit, H., Ouabadi, A., Khaldi, A., Hemmi, A., 2007. Late Panafrican evolution of the main Hoggar fault zones: Implications of magnetic fabric study in the In Telloukh pluton (Tin Serririne basin, Algeria). Journal of African Earth Sciences 49, 211–221. doi:10.1016/j.jafrearsci.2007.09.004.
Henry, B., Derder, M.E.M., Bayou, B., Guemache, M.A., Nouar, O., Ouabadi, A., Djellit, H., Amenna, M., Hemmi, A., 2008. Inhomogeneous shearing related with rocks composition: evidence from a major late-Panafrican shear zone in the Tuareg shield (Algeria). Swiss Journal of Geosciences 101, 453–464. doi:10.1007/s00015-008-1262-4.
Henry, B., Liégeois, J.P., Nouar, O., Derder, M.E.M., Bayou, B., Bruguier, O., Ouabadi, A., Belhai, D., Amenna, M., Hemmi, A., Ayache, M., 2009. Repeated granitoid intrusions during the Neoproterozoic along the western boundary of the Saharan metacraton, eastern Hoggar, Tuareg shield, Algeria: an AMS and U–Pb zircon age study. Tectonophysics 474, 417–434. doi:10.1016/j.tecto.2009.04.022.
Hext, G., 1963. The estimation of second-order tensors, with related tests and designs. Biometrika 50, 353.
Horstwood, M.S.A., Foster, G.L., Parrish, R.R., Noble, S.R., Nowell, G.R., 2003. Common-Pb corrected in situ U–Pb accessory mineral geochronology by LA-MC-ICPMS. Journal of Analytical Atomic Spectroscopy 18, 837–846.
Hrouda, F., Chlupáčová, M., Rejl, L., 1971. The mimetic fabric in some foliated granodiorites as indicated by magnetic anisotropy. Earth Planetary Science Letters 11, 381–384.
Jelinek, V., 1978. Statistical processing of magnetic susceptibility measured in groups of specimens. Studia geophysica et geodaetica 22, 50–62.
Jelinek, V., 1981. Characterization of the magnetic fabric of rocks. Tectonophysics 79, 63–67.
King, R.F., 1966. The magnetic fabric of some Irish granites. Geological Journal 5, 43–66.
Kratinová, Z., Schulmann, K., Edel, J.B., Ježek, J., Schaltegger, U., 2007. Model of successive granite sheet emplacement in transtensional setting: Integrated microstructural and anisotropy of magnetic susceptibility study. Tectonics 26, TC6003. doi:10.1029/2006TC002035.
Le Goff, M., 1990. Lissage et limites d'incertitudes des courbes de migration polaire: pondération, des données et extension bivariate de la statistique Fischer. Comptes Rendus de l'Académie des Sciences, Paris 311 (II), 431–437.
Le Goff, M., Henry, B., Daly, L., 1992. Pratical method for drawing a VGP path. Physics of the Earth and Planetary Interior 70, 201–204.
Lelubre, M., 1952. Recherches sur la géologie de l'Ahaggar central et occidental (Sahara central). Bulletin de Service de la Carte Géologique de l'Algérie 22 (tome 1, 354 p., tome 2, 387p.).
Liégeois, J.P., 2005. The Pan-African evolution of the Tuareg shield, with reference to the Neoproterozoic granitoids and the Cenozoic volcanism. Séminaire de géologie et de métallogenie des massifs du Hoggar et des Eglab, Tamanrasset, Algérie.
Liégeois, J.P., Black, R., Navez, J., Latouche, L., 1994. Early and late Pan-African orogenies in the Aïr assembly of terranes (Tuareg shield, Niger). Precambrian Research 67, 59–66.
Liégeois, J.P., Navez, J., Hertogen, J., Black, R., 1998. Contrasting origin of post-collisional high-*K* calc-alkaline and shoshonitic versus alkaline and peralkaline granitoids. Lithos 45, 1–28.
Liégeois, J.P., Latouche, L., Boughrara, M., Navez, J., Guiraud, M., 2003. The LATEA metacraton (Central Hoggar, Tuareg shield, Algeria): behaviour of an old passive margin during the Panafrican orogeny. Journal of African Earth Sciences 37, 161–190.
Liégeois, J.P., Stern, R.J., 2010. Sr–Nd isotopes and geochemistry of granite-gneiss complexes from the Meatiq and Hafafit domes, Eastern Desert, Egypt: no evidence for pre-Neoproterozoic crust. Journal of African Earth Sciences 57, 31–40.
Ludwig, K.R., 2003. User's manual for Isoplot/3, a geochronological toolkit for Microsoft Excel. Berkeley Geochronology Center, Special Publication 14, 71 pp.
Lugmair, G.W., Marti, K., 1978. Lunar initial 143Nd/144Nd: differential evolution of the lunar crust and mantle. Earth Planetary Science Letters 39, 349–357.
Nelson, B.K., Depaolo, D.J., 1985. Rapid production of continental crust 1.7–1.9 by ago: Nd isotopic evidence from the basement of the North American midcontinent. Geological Society of America Bulletin 96, 746–754.
Neves, S.P., Bruguier, O., Vauchez, A., Bosch, B., da Silva, J.M.R., Mariano, G., 2006. Timing of crust formation, deposition of supracrustal sequences and Transamazonian and Brasiliano metamorphism in the East Pernambuco belt (Borborema Province, NE Brazil): Implications for Western Gondwana assembly. Precambrian Research 149, 197–216.
Njanko, T., Nédélec, A., Kwékam, M., Siqueira, R., Estaban, L., 2009. The emplacement and deformation of the Fomopea pluton: Implications for the Pan-African history of Western Cameroon. Journal of Structural Geology. doi:10.1016/j.jsg.2009.12.007.
O'Reilly, W., 1984. Rock and Mineral Magnetism. Blackie, Chapman and Hall edit, Glasgow.
Pearce, J.A., 1982. Role of the Sub-continental Lithosphere in Magma Genesis at Active Continental Margins. Continental Basalts and Mantle Xenoliths. Shiva Publication, Cheshire, UK. pp. 230–249.
Pignotta, G.S., Benn, K., 1999. Magnetic fabric of the Barrington Passage pluton, Meguma Terrane, Nova Scotia: a two-stage fabric history of syntectonic emplacement. Tectonophysics 307, 75–92.
Steiger, R.H., Jäger, E., 1977. Subcommission on geochronology: convention on the use of decay constants in geo- and cosmochronology. Earth Planetary Science Letters 36, 359–362.
Sun, S.S., 1980. Lead isotopic study of young volcanic rocks from mid-ocean ridges, ocean islands and islands arcs. Philosophical Transactions of the Royal Society London A297, 409–445.
Taylor, S.R., Mc Lennan, S.M., 1985. The Continental Crust: Its Composition and Evolution. Blakwell, Oxford. 312 pp.
Tikoff, B., Teyssier, C., 1992. Crustal-scale, en-echelon "P-shear" tensional bridges: a possible solution to the batholith room problem. Geology 20, 927–930.
Tomezzoli, R.N., McDonald, W.D., Tickyj, H., 2003. Composite magnetic fabrics and S–C structure in granitic gneiss of Cerro de los Viejos, La Pampa province, Argentina. Journal of Structural Geology 25, 159–169.
Veksler, I.V., Dorfman, A.M., Kamenetsky, M., Dulski, P., Dingwell, D.B., 2005. Partitioning of lanthanides and Y between immiscible silicate and fluoride melts, fluorite and cryolite and the origin of the lanthanide tetrad effect in igneous rocks. Geochimica et Cosmochimica Acta 69, 2847–2860.
Vialon, P., Guérangé, B., 1959. Geological map "Mont du Métal" – "Mission hélicoptère 1958–59". Bureau de Recherches Minières de l'Algérie.
Wiedenbeck, M., Allé, P., Corfu, F., Griffin, W.L., Meier, M., 1995. Three natural zircon standards for U–Th–Pb, Lu–Hf, trace element and REE analyses. Geostandards Newsletter 19, 1–23.
Zeghouane, H., 2006. Pétrologie, géochimie, géochimie isotopique et géochronologie Rb/Sr du massif granitique d'Arirer (terrane Aouzegueur, Hoggar oriental) Algérie. Th. Magister Univ. Sc. Technologie Houari Boumédiène, Alger.
Zeghouane, H., Azzouni-Sekkal, A., Liégeois, J.P., 2008. Pétrologie et géochronologie des granitoïdes du massif d'Arirer, (Aouzegueur, Hoggar oriental, Algérie). Abstract, 22th Colloquium of African Geology, Tunis, Tunisia, p. 259.